NASA/CR—2004-213410

The Performance of a Subsonic Diffuser Designed for High Speed Turbojet-Propelled Flight

Bruce J. Wendt
Modern Technologies Corporation, Middleburg Heights, Ohio

December 2004

The NASA STI Program Office . . . in Profile

Since its founding, NASA has been dedicated to the advancement of aeronautics and space science. The NASA Scientific and Technical Information (STI) Program Office plays a key part in helping NASA maintain this important role.

The NASA STI Program Office is operated by Langley Research Center, the Lead Center for NASA's scientific and technical information. The NASA STI Program Office provides access to the NASA STI Database, the largest collection of aeronautical and space science STI in the world. The Program Office is also NASA's institutional mechanism for disseminating the results of its research and development activities. These results are published by NASA in the NASA STI Report Series, which includes the following report types:

- TECHNICAL PUBLICATION. Reports of completed research or a major significant phase of research that present the results of NASA programs and include extensive data or theoretical analysis. Includes compilations of significant scientific and technical data and information deemed to be of continuing reference value. NASA's counterpart of peer-reviewed formal professional papers but has less stringent limitations on manuscript length and extent of graphic presentations.

- TECHNICAL MEMORANDUM. Scientific and technical findings that are preliminary or of specialized interest, e.g., quick release reports, working papers, and bibliographies that contain minimal annotation. Does not contain extensive analysis.

- CONTRACTOR REPORT. Scientific and technical findings by NASA-sponsored contractors and grantees.

- CONFERENCE PUBLICATION. Collected papers from scientific and technical conferences, symposia, seminars, or other meetings sponsored or cosponsored by NASA.

- SPECIAL PUBLICATION. Scientific, technical, or historical information from NASA programs, projects, and missions, often concerned with subjects having substantial public interest.

- TECHNICAL TRANSLATION. English-language translations of foreign scientific and technical material pertinent to NASA's mission.

Specialized services that complement the STI Program Office's diverse offerings include creating custom thesauri, building customized databases, organizing and publishing research results . . . even providing videos.

For more information about the NASA STI Program Office, see the following:

- Access the NASA STI Program Home Page at ***http://www.sti.nasa.gov***

- E-mail your question via the Internet to help@sti.nasa.gov

- Fax your question to the NASA Access Help Desk at 301–621–0134

- Telephone the NASA Access Help Desk at 301–621–0390

- Write to:
  NASA Access Help Desk
  NASA Center for AeroSpace Information
  7121 Standard Drive
  Hanover, MD 21076

NASA/CR—2004-213410

The Performance of a Subsonic Diffuser Designed for High Speed Turbojet-Propelled Flight

Bruce J. Wendt
Modern Technologies Corporation, Middleburg Heights, Ohio

Prepared under C80054A

National Aeronautics and
Space Administration

Glenn Research Center

December 2004

Acknowledgments

The author is in gratitude for the initial technical guidance and support provided by A. Robert Porro, Raytheon. A special thanks to Tony Nerone for his dedicated effort at the mechanical design of the diffuser and supporting facility, and for his many trips to the fabrication shops. Technical advocacy and programmatic support were well-provided for by Dr. Ken Suder, representing NASA's Propulsion Research and Technology program, and Tom Biesiadny, NASA Glenn. Technical support on inlet design issues and inlet design computations were provided by J. Dave Saunders and Franco Frate, NASA Glenn and QSS Group, Inc., respectively. Test engineering support was provided for by Dave Haydu and Phil Blumenthal, QSS Group, Inc. Test mechanical support was provided by Robert McCluskey and Gerald Hurd, NASA Glenn.

Available from

NASA Center for Aerospace Information
7121 Standard Drive
Hanover, MD 21076

National Technical Information Service
5285 Port Royal Road
Springfield, VA 22100

Available electronically at http://gltrs.grc.nasa.gov

The Performance of a Subsonic Diffuser Designed for High Speed Turbojet-Propelled Flight

B. J. Wendt*
Modern Technologies Corporation
Middleburg Heights, Ohio 44130

Abstract

An initial-phase subsonic diffuser has been designed for the turbojet flowpath of the hypersonic x43B flight demonstrator vehicle. The diffuser fit into a proposed mixed-compression supersonic inlet system and featured a cross-sectional shape transitioning flowpath (high aspect ratio rectangular throat-to-circular engine face) and a centerline offset. This subsonic diffuser has been fabricated and tested at the W1B internal flow facility at NASA Glenn Research Center. At an operating throat Mach number of 0.79, baseline Pitot pressure recovery was found to be just under 0.9, and DH distortion intensity was about 0.4 percent. The diffuser internal flow stagnated, but did not separate on the offset surface of this initial-phase subsonic diffuser. Small improvements in recovery (+0.4 percent) and DH distortion (–32 percent) were obtained from using vane vortex generator flow control applied just downstream of the diffuser throat. The optimum vortex generator array patterns produced inflow boundary layer divergence (local downwash) on the offset surface centerline of the diffuser, and an inflow boundary layer convergence (local upwash) on the centerline of the opposite surface.

Introduction and Background

This report details an effort to develop the subsonic diffuser of a supersonic inlet system undergoing design for the x43B hypersonic flight demonstrator vehicle. This study was begun late in 2000. At that time, an initial layout of the x43B detailing the internal structure and flowpath overall dimensions had been prepared by engineers at Boeing.[1] Figure 1 is a sketch showing 4 different views of the x43B flight demonstrator as detailed in the initial Boeing layout. The x43B reaches hypersonic speed (a flight Mach number in excess of about 6) through the use of a "turbine-based combine cycle" or "TBCC" propulsion system. This system consists of a spanwise row of 4 turbojets occupying the upper portion of the vehicle, and a dual-mode ramjet/scramjet duct occupying the lower portion of the vehicle. The 4 turbojets are fed by a supersonic inlet section (partitioned into 4 separate channels) and exhaust to 4 nozzles separated by splitter plates. This turbojet system is referred to as the "low-speed" system since it is used to propel the vehicle from take-off conditions to a flight Mach number of about 4. The low-speed portion of the x43B propulsion system is illustrated by the unshaded regions of figure 1. Above a flight Mach number of about 4, the turbojets are shut down and the supersonic inlet channels feeding the low-speed flowpath are closed off using a hinged cowl-door on the vehicle forebody. At this condition, the vehicle is solely propelled by the "high speed" dual-mode ramjet/scramjet, indicated by the dark shading in figure 1.

In the initial Boeing layout, the supersonic inlet concept was purposefully kept simple: the hinged cowl-door was to be used to vary the airflow to the engine (as required by the demands of operating over the large range of flight Mach numbers from 0 through 4) and a downstream isolator duct was to be used for shock stability. Such an inlet system has the benefit of design simplicity, but would have likely proved unworkable due to the difficulty of meeting the airflow pressure recovery and distortion demands of the downstream turbojets. Primarily for this reason, an effort was initiated at NASA Glenn Research Center (GRC) to refine the supersonic inlet design of the low-speed propulsion system. A mixed-compression supersonic inlet consisting of a supersonic diffuser, a variable area bled throat, and a subsonic diffuser was proposed. This inlet concept has historically been a focus of NASA GRC research. Refined analysis and design tools are available to experienced GRC inlet engineers, and a large number of mixed-compression inlets have been successfully developed to provide the high recovery, low distortion, and operative stability characteristics required by modern turbojet-based propulsion.[2-6] This is most recently demonstrated by the development of the high performance two-dimensional bifurcated (2DB) supersonic inlet for the High Speed Research (HSR) program.[7-8] Figure 2 summarizes the efforts conducted to establish a mixed compression inlet within the framework established by the initial Boeing layout.[9] Reference 9 provides a good summary of the many considerations of the overall supersonic inlet design process followed, and details the specific analysis tools and computations performed in the study. This report focuses on the development of the subsonic diffuser, a portion of the overall inlet program which used both analysis and experiments to investigate the performance characteristics of a representative "TBCC-class" subsonic diffuser.

Figure 2 illustrates some of the challenges faced when designing effective subsonic diffusion for the x43B low-speed flowpath. The throat plane (the location of minimum

*NASA Resident Research Engineer at Glenn Research Center.

flow area and the boundary between the supersonic and subsonic diffuser) is a high aspect ratio rectangle which has its long dimension following the spanwise coordinate of the flow path. This rectangular shape transitions to a circular engine face over the axial length of the diffuser. In addition, the centerline locations of the throat and engine face are offset from each other by a certain distance yielding an S-shaped centerline for the diffuser. The combination of transitioning flow area and centerline offset are known to produce secondary flows and associated flow separation. These naturally occurring flow phenomena can potentially reduce diffuser pressure recovery and increase flow distortion. Another aggravating problem inherent in the x43B design is the likely ingestion of a thick forebody boundary layer into the inlet. As figure 2 indicates, this forebody boundary layer is ingested into the inlet on the upper surface of the diffuser. The upper surface of the subsonic diffuser also requires the most flow turning, and so a thick and sluggish boundary layer here will be much more likely to separate.

Our planned approach to subsonic diffuser development had it occurring in "phases" with each phase defined by a specific diffuser model or test article. Our "first phase" diffuser was designed to possess all of the geometric challenges discussed above, and to have it fit within the overall dimensions specified by the initial Boeing layout and subsequent supersonic diffuser design. Further considerations of its detailed design are discussed below. Our objective was to design, fabricate, and test this diffuser in a baseline configuration (without flow control) and to use it as a testbed to develop flow control techniques to possibly improve its baseline pressure recovery and distortion characteristics. The lessons learned here, we reasoned, would apply as we proceeded in the development to later phases. Since the internal design of the x43B, the x43B low-speed flow path, and the airflow requirements of the x43B turbojets were initially rather nebulous (but undergoing development as well) these later phases of subsonic diffuser development would incorporate modifications to the first phase design to account for the refining vehicle and propulsion system designs. The additional flow challenge of an ingested forebody boundary layer was also a consideration for a future phase of this work. Let's now proceed with a description of the first phase subsonic diffuser detailed design.

The Subsonic Diffuser Design

Detailed design of the subsonic diffuser starts with a consideration of the engine sizing and airflow requirements. Three partially-developed candidate engines were under consideration for use in the x43B at the time this study got underway. Of direct interest to us is the variation in engine corrected flow (and associated engine face Mach number) versus flight Mach number. In general terms, as the flight Mach number increases the airflow to the engine decreases. The drop in turbojet flow capacity and associated thrust is due partly to the relative intolerance of the engine core to the influx of the hot airstream, where total temperatures can be in excess of 1200 °F. This consideration, of course, is built into the design of the TBCC system. The decreasing level of thrust provided by the turbojets is offset by the operation of the ramjet/scramjet near the transition Mach number. The ratio of engine face area to throat area is known simply as the diffuser "area ratio". Due to reasons of mechanical complexity and associated cost it was not possible to build and test a diffuser with variable throat area; a single value of throat height h had to be settled upon. Thus, in the interest of obtaining a diffuser geometry which would require the greatest conceivable amount of subsonic diffusion (and thereby the greatest challenge to good performance), the largest of the three engine concepts (D = 19 inches) was matched with the lowest engine face Mach number at the transition flight Mach number of 4 ($M_{ef} \approx 0.07$). Computations were conducted to determine throat height[9] and assumed the flow exiting the supersonic diffuser had a Mach number in the transonic range $1.3 \geq M_t \geq 1.5$, the presence of an ingested forebody boundary layer, a terminal shock, and porous normal bleed at the throat location. One geometry option in the Boeing layout specified a constant subsonic diffuser width (span dimension) equal to D, over the entire axial length of the diffuser. When holding to this specification, the throat height was determined to be $h \approx 0.079$D. Figure 2 depicts the throat cross-section against the downstream engine face plane. The area ratio at this flow condition is nearly 10. An area ratio of 10 is much larger than that typically encountered in subsonic diffusers and thus represents the greatest challenge to good performance from this design. Working in our favor, however, is the overall axial length available for the subsonic diffuser. From figure 2 we see that this distance is 7.620D. When the effective conical angle of diffusion is calculated for this flow path, we discover that it is below 8°, a value recommended for separation-free subsonic diffusers.[10-12] In fact, the value $\theta_{eff} \approx 5°$ determined is very similar to the high performance subsonic diffusers designed for the HSR program, and this fact will be used to define the area schedule (cross-sectional area versus axial distance) of the diffuser below.

Primarily for the sake of design simplicity, a constant span width (=D) was chosen. As mentioned previously, this design option was part of the original Boeing layout. The design was further simplified by increasing the diffuser centerline offset from 0.378D to 0.461D. This allowed the bottom surface centerline of the diffuser to be horizontal (with no curvature) from the throat to the engine face location. Considerations of fluidic operation lead to a diffuser design composed of three parts; an inflow two-dimensional diffuser section designed to provide terminal shock stability, a three-dimensional diffuser section designed to transition the duct cross-section from rectangular to circular, and a constant area spool section designed to

contain a bypass air cavity and system for overall inlet operational stability. Figure 3 is an orthographic sketch of the resulting detailed diffuser aerodynamic design showing the lofted lines for one half (the left half) of the diffuser. The three diffuser sections are now discussed in detail.

2D Inflow Diffuser Section

A centerline cut-away view of the 2D inflow diffuser section is illustrated in figure 4. This diffuser section begins with the throat plane: a rectangle of width D, a height of h = 0.079D, and 4 sharp (90°) corners. It is here where the terminal shock must sit (under normal operating conditions) in stable fashion. The terminal shock will seek a clearly defined location of minimum cross-sectional area. We made the throat plane a clearly defined location of minimum area by canting the upper surface of the 2D inflow section by 2° over its entire axial length of 1/2D = R. The four sharp corners of the throat plane transition to the rounded corners of the exit plane of the 2D inflow section over the axial distance R. These rounded corners have a shape described by the equations used to loft the 3D transitioning diffuser section discussed next.

Transitioning 3D Diffuser Section

As indicated in figure 3, the 3D transitioning diffuser section changes its cross-sectional shape from a near-rectangle (the 2D inflow diffuser section rectangular exit plane with rounded corners) to a circle over its hefty axial length of 13.240R. The exact description of its cross-sectional shape is "super-elliptical". A dual coordinate system is used to fully describe this shape and its axial or streamwise transition. Figure 5 defines this dual coordinate system. Figure 5 is a side (centerline cut-away) view of the diffuser from the throat plane into the upstream portion of the 3D transitioning section. The exit plane of the 2D inflow section is the "initial plane" of the 3D transitioning section. The coordinates x/R, y/R, and z/R represent the base Cartesian coordinate system. The origin of this three dimensional base coordinate system is the central point of the initial plane (the point through which the diffuser centerline passes). This centerline (which corresponds precisely with the centerline of the 3D transitioning section) was defined to be a fifth order polynomial in terms of x/R. The constants in this polynomial were found using the given offset and setting the first and second spatial derivatives equal to zero at the initial plane (x/R = 0.000) and exit plane (x/R = 13.240) boundaries. The resulting matrix of equations was solved for the constants and the centerline equation was found to be:

$$cl\,(x/R) = 0.0038932\cdot\left[\frac{x}{R}\right]^3 - 0.0004411\cdot\left[\frac{x}{R}\right]^4 + 0.0000133\cdot\left[\frac{x}{R}\right]^5 \tag{1}$$

The super-elliptical diffuser cross-section was defined using a two-dimensional coordinate system orthogonal to the centerline defined by equation (1). The terms "y'/R" and "z'/R" represent this orthogonal coordinate system (see fig. 5). The super-elliptical cross-sections were defined by the following equation:

$$\frac{z'}{R} = b0\cdot\left[1.0 - \left[\frac{y'}{R}\right]^n\right]^{1/n}. \tag{2}$$

The variables $b0$ and n are also fifth order polynomials in terms of x/R and are found to be:

$$\begin{aligned} b0\,(x/R) &= 0.0964000 + 0.0038932\cdot\left[\frac{x}{R}\right]^3 - \\ &\quad 0.0004411\cdot\left[\frac{x}{R}\right]^4 + 0.0000133\cdot\left[\frac{x}{R}\right]^5, \\ n\,(x/R) &= 30.000000 - 14.293807\cdot\left[\frac{x}{R}\right] + \\ &\quad 2.9699493\cdot\left[\frac{x}{R}\right]^2 - 0.3074365\cdot\left[\frac{x}{R}\right]^3 + \\ &\quad 0.0157627\cdot\left[\frac{x}{R}\right]^4 - 0.0003200\cdot\left[\frac{x}{R}\right]^5. \end{aligned} \tag{3}$$

The constants in the expression for $b0$ were determined from the requirement that the diffuser bottom surface centerline is horizontal (with no curvature). The super-elliptical exponent, n(x/R), controls the nature of the diffuser corners. A large value of n (for example n = 30) gives the diffuser cross-section tight radius corners, a value of n close to 2 provides a diffuser cross-section that is circular. The constants in the expression for n were determined from an iterative fitting procedure to the desired cross-sectional area schedule of the diffuser. As was mentioned earlier, θ_{eff} was found to have a value similar to those for subsonic diffusers designed for the HSR program. One diffuser in particular, the so-called td118[13] was designed (using computational analysis) to provide stall-line separation-free flow. It was found in subsequent experimental testing[14] that this diffuser did indeed perform near the stall line. Figure 6 illustrates the area schedule for the td118 nondimensionalized in a form suitable for our current use. The constants for n (see eq. (3) above) were simply adjusted until the area schedule of the 3D

transitioning diffuser section matched that of the td118 diffuser.

Figure 7 is an axial cut-away view of the diffuser model and is drawn in correct proportion. Figure 8 depicts the 3D transitioning diffuser cross-sectional profiles at six axial stations spanning the length of this diffuser section.

Constant Area Section

A constant area pipe or "spool" section of axial length 1.000R comprises the downstream portion of the diffuser. This section of the diffuser was designed to accommodate a possible (future phase work) circumferential bypass air cavity often used for the purpose of shock-stable operation in mixed compression inlet systems.

The diameter of the exhaust line used to pull the airstream through the diffuser model was 12.0 inches. Since the diameter of the proposed x43B turbojet was 19 inches, the ratio of 12/19 defines the scale of the model diffuser. Figure 9 illustrates the area schedule of the diffuser composed of the three sections discussed above, and also illustrates the results of one-dimensional compressible flow analysis for interior (core) Mach number versus x/R. In this analysis, the throat Mach number was assumed to be 0.786 (subsonic flow following a terminal shock in the Mach 1.3 airstream exiting the supersonic diffuser) and the upstream total conditions were those of a standard atmosphere. The throat Mach number condition of 0.786 is hereafter known as the "reference flow condition". The step change in wall slope (from 2° to 0°) at the boundary between the 2D inflow diffuser section and the 3D transitioning diffuser section produces a corresponding "kink" in the Mach number variation with x/R.

Facilities and Procedures

Test Section

The diffuser was fabricated in two halves from "Ren Shape", a dense plastic material. The interior flow surfaces were machined into the Ren Shape halves, and an outer cylindrically-shaped skin of aluminum alloy was epoxied onto the interior plastic core. Figure 10 is an axial cut-away view of the diffuser model showing some of the attached upstream and downstream ductwork. To determine the axial pressure profile (for inferring diffuser interior flow conditions) two streamwise rows of surface static pressure taps ran the length of the diffuser on the top and bottom surface centerlines. Three spanwise rows of vortex generator mounting "stations" were provided at locations x/R = 3.0, 4.0, and 5.0. At each of these locations there were 18 equally-spaced mounting ports for vortex generators, 9 on the top and 9 on the bottom surface. The vortex generators were airfoils having a NACA 0009 profile, split in half. These were machined from stainless steel. In the absence of a vortex generator, each mounting port was filled with a surface plug. This plug was machined to provide a surface-flush fit. The plugs or vortex generators were mounted on long threaded rods fed through steel tubing epoxied into the diffuser. The vortex generator airfoils could be set to any desired angle-of-attack α on the flow surface. Figure 11 illustrates a spanwise cut-away view of the diffuser model at the upstream vortex generator mounting station (x/R = 3.0), and diagrams the vortex generator airfoil. In order to access the flow surface to change out the vortex generator patterns, the diffuser was split into top and bottom halves. With a mass in excess of 700 pounds, an overhead crane was required to lift the top surface off of the bottom surface. A flange running the length of the model was provided as a means to attach the halves together for testing.

A duct section referred to as the "inflow duct" (see fig. 10) was mounted just upstream of the diffuser throat plane. It was used to set the throat Mach number and for conducting detailed Pitot pressure surveys of the boundary layer entering the diffuser. The inflow duct had a constant cross-sectional area in the precise shape of the diffuser throat and an axial length of 5.5 inches. A circumferential ring of surface static pressure taps was used to determine the inflow static pressure ratio and corresponding inflow core Mach number. There were 4 sealed slots evenly spaced about the circumference of the inflow duct. These were used to provide access for the boundary layer Pitot probe. Figure 12 illustrates the boundary layer survey mechanism. A goose-necked stainless steel tube with a flattened tip was traversed along the normal (z) axis using a Newport 2 inch actuator. The survey resolution was approximately 40 points over a normal distance of about 0.75 inches.

Figure 10 depicts an axial cut-away view of the instrumentation duct. This duct was mounted just downstream of the diffuser model. It had a 12 inch inner diameter and contained a 99-tube Pitot rake. The cross-stream plane into which the Pitot probe tips are located is referred to as the "Aerodynamic Interface Plane" or "AIP". Figure 13 is a cross-stream view of the AIP Pitot rake. There are a total of eight radial arms spaced 45 degrees apart. Seven arms contain 12 equally-spaced Pitot probes along the radial coordinate. Arm number 8 has 12 equally-spaced Pitot probes (in the same radial positions as on the other 7 arms) with an additional 3 Pitot probes near the center (r = 0). One of these extra probe tips is precisely located on the AIP centerline. Although this rake was designed to be clocked at any circumferential position, the orientation shown in figure 13 was the only position used to acquire data in this study. Pitot and static pressures were recorded with an electronically-scanned pressure transducer system ("ESP"). All pressures recorded with the ESP transducers are certain to within ± 15 Pascals.

Facility

Figure 14 illustrates the diffuser model and supporting ductwork as it appeared mounted within the overall test

facility. The air that moved through the facility originated from the surrounding test cell and so the total conditions were always those of the ambient atmosphere. A large cylindrical upstream plenum contained screens and a honeycomb to reduce the incoming turbulence intensity. A transitioning bellmouth smoothly accelerated the flow from the plenum conditions to the throat conditions. This bellmouth had a circular upstream aperture and a downstream (exit) aperture that matched the throat plane shape of the inflow duct and the diffuser. The flow through the test section was driven by a downstream vacuum exhaust. This was maintained in continuous fashion (for steady state flow) by compressors located on-site at NASA Glenn. This flow was controlled through the use of two exhaust butterfly valves, a main line 12 inch valve, and a bypass line 4 inch valve. For this test, diffuser flow and performance data was recorded for throat Mach numbers in the range $0.1 \le M_t \le 0.8$. This range produced a maximum mass flux of about 3.6 lbm/sec and a maximum Reynolds number (based on throat flow conditions) of about 4,000,000.

Diffuser Performance Descriptor Definition

Due to the nature of the instrumentation used at the AIP (see fig. 13) diffuser performance is calculated using *Pitot* pressure, as opposed to *total* pressure. Pitot pressure is defined to be the pressure sensed by bringing the fluid to rest along the axial component of flow, as was done using the previously described AIP Pitot rakes. Total pressure is the pressure sensed by bringing the fluid to rest along the local direction of flow, and can be calculated from measurements obtained using multi-port pressure probes (five or seven-hole probes). The diffuser performance descriptors evaluated in this study are area-averaged Pitot pressure recovery and Pitot pressure distortion intensity. An area-average of a quantity β over an annular section of angular extent $\Delta\theta = b\text{-}a$ and radial extent $\Delta r = d\text{-}c$ is defined as:

$$\overline{\beta}(a,b:c,d) = \frac{\int_a^b \int_c^d \beta\, r\, dr\, d\theta}{\int_a^b \int_c^d r\, dr\, d\theta}. \qquad (4)$$

Define P to be the nondimensional pressure obtained by dividing the Pitot pressure p_p, measured at any point in the AIP, by the reference Pitot pressure, or:

$$P \equiv p_p \,/\, p_{p\,ref}\,. \qquad (5)$$

In equation (5) $p_{p\,ref}$ represents the reference Pitot pressure. The reference Pitot pressure was obtained in the upstream flow conditioning plenum through the use of a Pitot probe. Area-averaged Pitot pressure recovery, or AAPPR, is defined from equation (4) by letting $\beta = P$, $a = 0$, $b = 2\pi$, $c = 0$, and $d = \mathrm{R}$ (AIP radius = 5 inches). Following the geometry of the AIP Pitot rakes shown in figure 13, equation (4) is reduced to:

$$\overline{P}(0,2\pi:0,R) = \sum_{i=1}^{8}\sum_{j=1}^{13} P_{ij}\, dA_j \,/\, \pi R^2\,, \qquad (6)$$

where A_j represents the area element of incremental radial thickness = 0.440 inches, incremental angular extent = 45 degrees, and centered on the Pitot port at location r_j measured from duct center ($r = 0$). Equation (6) is our expression for AAPPR.

A general description of the distortion intensity is provided by the so-called "DH" descriptor defined as:

$$DH = \frac{P_{p\max} - P_{p\min}}{\overline{P}(0,2\pi:0,R)}. \qquad (7)$$

In this expression P_{pmax} and P_{pmin} are the maximum and minimum values of nondimensional Pitot pressure acquired, respectively.

Results

Throat Flow Conditions

The throat flow conditions were evaluated with a circumferential ring of surface static pressure taps and the boundary layer survey apparatus. Both of these measurement systems were located in the throat of the diffuser. Throat core Mach numbers M were varied over the range $0.10 \le M \le 0.80$ with corresponding Reynolds numbers (based on throat width w) $800{,}000 \le Re \le 4{,}300{,}000$.

Figure 15 is an illustration of throat boundary layer velocity profiles derived from Pitot pressure measurements taken at M = 0.400, 0.500, 0.600, 0.700, and 0.786. These measurements were recorded with the flattened boundary layer Pitot probe traversed in the upper left throat survey port. Figure 15 also tabulates the calculated values of Coles[15] compressible integral boundary layer parameters, defined as follows:

Displacement Thickness

$$\partial^* = \int_0^\infty \left(1 - \frac{\rho u}{\rho_\infty u_\infty}\right) dy, \qquad (8)$$

Momentum Thickness

$$\Theta = \int_0^{\infty} \frac{\rho u}{\rho_{\infty} u_{\infty}} \left(1 - \frac{u}{u_{\infty}}\right) dy, \qquad (9)$$

Shape Factor

$$H = \partial^* / \Theta. \qquad (10)$$

In these expressions the "∞" designation represents the core flow conditions of the throat. Calculated values of boundary layer thickness δ, friction velocity u_τ, wall shear stress τ_w, and fluidic throat blockage (in percent) are also listed.

Diffuser Baseline Results

The qualitative nature of the baseline diffuser near-surface flows was investigated using a fluorescent oil flow technique. The diffuser was split into two halves and drops of viscous oil containing powdered fluorescent dye were applied in a regular grid on the top and bottom surfaces of the diffuser in the region immediately downstream of the throat. The oil was viscous enough (and surface tension high enough) so that the drops would hold their shape (under a no-flow condition) against gravity for periods of time as long as 30 minutes. After the grid of oil drops was applied, the duct was reassembled and brought quickly up to the reference baseline flow condition (M_t = 0.786). The diffuser was run at this condition for about 10 minutes. During this time, frictional forces drew the oil drops into lines or "streaks". The length and direction of each streak relates to the local skin friction magnitude and direction. After running the tunnel steady state for the 10 minute period, the tunnel was shut down, and the diffuser disassembled. The resulting streak pattern was photographed under ultra-violet lighting, and the oil dye pattern transmitted (in two-dimensional form) to paper by direct contact. The resulting patterns are illustrated in figure 16. The flow near the bottom surface is seen to be attached throughout. The flow is primarily in the axial component, with the cross-stream component being rather small. The one notable exception to this occurs near the sidewall region of the diffuser, where the influence of the sharp 90° upstream corners has led to a slight divergence or "spreading" of the flow. The flow near the top surface is also primarily in the axial component, but a rapid deceleration is apparent as the upper surface turns away from the primary (axial) direction of the flow. The flow is seen to stagnate completely at $x/R \approx 5.0$. However, no backflow or recirculation appears.

Axial profiles of surface static pressure for the baseline reference flow condition are illustrated in figure 17. This figure illustrates characteristics common to all baseline static pressure results for the diffuser. With the exception of one data point (the surface static pressure located at the exit of the inflow 2d diffuser section), the axial profile of surface static pressure on the top surface centerline is identical to that occurring on the bottom surface centerline. There are two distinct steep rises in static pressure coinciding with two initial regions of area expansion in the diffuser. The first (and steepest) occurs in the 2d inflow diffuser section. Recall from the area curve (fig. 9) that this diffuser section has constant wall slope and terminates suddenly at the point where the transitioning 3d diffuser section begins. The constant wall slope of the 2d inflow diffuser upper surface also terminates (and is zeroed) at the start of the transitioning 3d diffuser section. This is reflected in the slope of the pressure rise (the magnitude of dP/dx as indicated in fig. 17) which goes from its maximum value to nearly zero as is seen by the "kink" in the static pressure curve at x/R ≈ 1.0. Although this discontinuity is very pronounced in figure 17, no corresponding surface flow anomalies were observed at this position (on either the top or bottom surfaces) in the oil flow results (see fig. 16). The second steep rise in static pressure occurs as the transitioning 3d diffuser section opens up. This rise terminates at x/R ≈ 5.0, which coincides with the axial location at which the surface oil flow was seen to stagnate on the upper surface. The final rise in pressure occurs gradually and in approximately linear fashion from x/R = 5.0 to x/R = 13.0. The static pressure recovery at the diffuser exit for the reference flow condition is a little less than 0.90 (from fig. 17). It is interesting to note that about 91 percent of the static pressure recovery of the diffuser is obtained in the first one-third of the duct. Over this initial one-third of its axial length, the duct diffuses to about 3 times its initial cross-sectional area. The final 9 percent of the static pressure recovery is obtained over the downstream two-thirds of its axial length where the duct diffuses an additional 151 percent, or to about 10 times its initial cross-sectional area. Figure 18 illustrates the axial surface static pressure profiles on the diffuser top surface for the cases of four throat Mach numbers spanning the range from 0.00 to 0.80. For future reference, each profile is labeled with an identifying "reading number" descriptive of its location in the test matrix. These axial profiles are similar to that observed for the reference flow condition. This figure also illustrates the sensitivity of the diffuser static pressure recovery to throat Mach number. This sensitivity will also be apparent in the results for Pitot pressure recovery, which are now described.

The Pitot pressure patterns for the reading numbers illustrated in the previous baseline static pressure ratio results (readings 0043, 0045, 0048, 0489, and 0052) are shown in figure 19. Included on this plot are the corresponding Pitot pressure recovery (AAPPR) and DH distortion intensity descriptors calculated from the rake data used to produce each pattern. At the reference flow condition (M_t = 0.79) the Pitot pressure recovery is a little under 0.900. The DH distortion has a remarkably low value of about 0.4 percent at the reference flow condition. This result reflects the miniscule variation observed in Pitot pressure across the AIP. In the case of reading 0052 (the pattern in the lower right corner of fig. 19), for example, Pitot pressure ratio varies

between about 0.8920 and 0.8955. At throat Mach numbers less than 0.80, this variation is even smaller. Figure 20 illustrates the variation in AAPPR versus throat Mach number for all 47 baseline diffuser data points (reading numbers) recorded. Figure 21 illustrates the corresponding variation in DH versus throat Mach number for the same set of 47 reading numbers.

Diffuser with Flow Control Results

Flow control was applied to counter adverse flow development in the baseline diffuser following a procedure outlined in reference 16. In this reference, the countering element to adverse flow was the convective influence created by vortices shed from delta-vane vortex generators mounted at an upstream location in the diffuser near the throat. In the baseline diffuser of this previous study, regions of sluggish fluid near the top and bottom of the AIP occurred through boundary layer development on the diffuser top and bottom surfaces. This resulted simply from the geometry of the diffuser; both top and bottom surfaces turned away from the axial component of the flow, with the adverse pressure gradient enhancing the tendency for the boundary layer to thicken on these surfaces. The strategy behind vortex generator flow control for this case was to get the core stream to turn and better follow the contours of the diverging surfaces. Figure 22 diagrams how this was accomplished and understood. The pair of vortex generators on the upper left of the figure produces a “divergence” in the boundary layer, with the flow between vortices directed down towards the wall. The induced convection by the vortex pair forces the core stream down in response. If the slope of the wall between the vortices is turning down, the effect would be beneficial on the boundary layer development in the downstream diffuser (meaning that the boundary layer would thicken at a slower rate). Adding co-rotating neighbor vortices to either side of this pair (see the lower left portion of fig. 22) merely enhances this convective effect. Alternatively, if the vortex generators are set to produce a “convergence” in the boundary layer (right-hand side of fig. 22) the convection of the shed vortices deflects the core stream up and away from the wall. In the diffuser of reference 16 diverging pairs of large delta-vane vortex generators were positioned on the upper and lower surfaces in an attempt to reduce the boundary layer thickening and flow separation evident in the diffuser at the AIP. Placement was by trial-and-error iteration, with the results gauged by the total pressure recovery and distortion descriptors. Care was required in the pair placement; divergent pairs placed too close together would have a convergence region between them with (usually) detrimental effects. Following the placement procedure, refinements were attempted to optimize the diffuser total pressure recovery and/or distortion performance. These refinements included replacing each large vortex generator with smaller co-rotating multiples (as in the lower half of fig. 22) and varying the spacing between left and right vortex generators or their substitute co-rotating arrays.

Following the procedure outlined in reference 16, vortex generator arrays were developed to represent six different “convective strategies” for flow control in the current diffuser study. Forty-four individual array patterns representing these six strategies (or variants of these strategies) were tested. Figure 23 diagrams the convective nature of each strategy attempted. At the top left corner of figure 23 is the strategy termed “top surface divergence”. We can best understand this strategy by first referring to the diffuser diagrammed in figure 10. Since it is the top surface of the diffuser that turned away from the flow (thus causing the top boundary layer to stagnate first) we wanted the vortices to convectively turn the core flow in a direction that would follow this surface (“up”). The divergence created in the upper surface boundary layer by the vortex generators in the upper left of figure 23 did this. This favorable flow turning can also be accomplished by a convergence in the boundary layer on the lower surface. Thus this type of strategy is termed 'bottom surface convergence”. The combination of both strategies is also useful and is termed “top surface divergence - bottom surface convergence”. Other strategies attempted include “top surface divergence - bottom surface divergence”, “clockwise swirl”, and “counterclockwise swirl”. The number of individual array patterns tested representing each of these six strategies is listed on figure 23. In general terms, it was found that the large vortex generators used at the upstream station (x/R = 3.0) worked best. Use of the small and medium vortex generators at the two downstream mounting stations (x/R = 4.0 and 5.0) produced results not noticeably different from baseline results. The patterns of vortex generators producing the best recovery and distortion characteristics, and those producing the worst characteristics, are illustrated in figure 24. In corresponding fashion, figure 25 illustrates the AIP Pitot pressure ratio profiles for each vortex generator array pattern illustrated in figure 24.

The array pattern numbered 30 (clockwise swirl with 18 large vortex generators mounted at x/R = 3.0) produced the worst (lowest) measured Pitot pressure recovery (AAPPR = 0.8961). This result is essentially equivalent to the baseline result since the decrement of 0.06 percent in AAPPR is within the uncertainty of the measurement (AAPPR ± 0.0007). The strong flow asymmetry imposed by a full co-rotating array of clockwise-spinning vortices is evident in the Pitot pressure pattern and reflected in the large value of DH distortion, which is 57 percent higher than the baseline result.

The array pattern numbered 23 (top surface divergence - bottom surface divergence with 12 large vortex generators mounted at x/R = 3.0) produced the worst (highest) DH distortion result (DH = 0.0065), an amount which is 66 percent higher than the baseline result.

The array pattern numbered 42 (top surface divergence - bottom surface convergence with 12 large vortex generators mounted at x/R = 3.0) produced the best (highest) recovery result with an improvement 0.4 percent higher than the baseline AAPPR. As in all other cases with similar improvements in recovery, the DH distortion is also significantly improved (here with a value that is 25 percent lower than the baseline result).

The array pattern numbered 17 (top surface divergence - bottom surface convergence with 16 large vortex generators mounted at x/R = 3.0) produced the best DH distortion result with a value that is 32 percent lower than the baseline result.

The performance numbers quoted above are for the diffuser operating at the reference throat Mach number condition. Figure 26 illustrates these descriptor result comparisons for a throat Mach number range $0.70 < M_t < 0.80$. The performance improvements obtained from using the hybrid strategy of top surface divergence - bottom surface convergence is the most significant result of this study. Recall the geometry of the proposed x43B from figure 10. It is the top surface of the diffuser that turns away from the flow direction and so it is on the top surface that we find evidence for rapid downstream boundary layer thickening, with attendant losses in diffuser performance. There is one other problem, only briefly mentioned before, that will impact the use of vortex generator flow control to form the top surface flow divergence. *The x43B vehicle will likely ingest a forebody boundary layer that will add significantly to the boundary layer thickness on the upper surface.* This will diminish (or eliminate altogether) the effectiveness of the flow control provided by vortices generated by vortex generators embedded in this thick boundary layer. Thus the convergence of the boundary layer produced by vortex generators mounted on the lower surface (in accord with the optimum patterns diagrammed in figure 24) will likely be the key to effective flow control in the x43B subsonic diffuser. This author knows of no other situation in which effective flow control in a subsonic diffuser has been provided by an upstream boundary layer convergence applied in this manner.

Summary

An initial-phase subsonic diffuser has been designed for the turbojet flowpath of the hypersonic x43B flight demonstrator vehicle. The diffuser fit into a proposed mixed-compression supersonic inlet system and featured a cross-sectional shape transitioning flowpath (high aspect ratio rectangular throat-to-circular engine face) and a centerline offset. This subsonic diffuser has been fabricated and tested at the W1B internal flow facility at NASA Glenn Research Center. At an operating throat Mach number of 0.79, baseline Pitot pressure recovery was found to be just under 0.9, and DH distortion intensity was about 0.4 percent. The diffuser internal flow stagnated, but did not separate on the offset surface of this initial-phase subsonic diffuser. Small improvements in recovery and distortion were obtained from using vane vortex generator flow control applied just downstream of the diffuser throat. The optimum vortex generator array patterns produced inflow boundary layer divergence on the offset surface centerline of the diffuser, and an inflow boundary layer convergence on the centerline of the opposite surface.

Future Work

Work on the x43B subsonic diffuser was to continue under NASA's Next Generation Launch Technology (NGLT) program. A set of modifications were discussed for the next-phase diffuser design study. These included a possible reduction in diffuser area ratio and length. In addition, preparations for throat geometry variations and ingested forebody boundary layer simulation were initiated when NGLT started-up in mid-January of 2004. This work ceased abruptly in late-January of 2004 when the NGLT program (that portion of it representing hypersonic flight technology development) was cancelled. At this time, there are no plans to carry this work forward.

References

[1]The original layout is detailed in a Boeing document titled "TBCC Vehicle Design (HFX-TB3-A1). This document has a limited distribution. A more general description of the x43B demonstrator vehicle is found in a paper by Moses, P.L., Bouchard, K.A., Vause, R.F., Pinckney, S.Z., Ferlemann, S.M., Leonard, C.P., Taylor, L.W., Robinson, J.S., Martin, J.G., Petley, D.H., and Hunt, J.L., "An Airbreathing Launch Vehicle Design with Turbine-Based Low-Speed Propulsion and Dual-Mode Scramjet High-Speed Propulsion," AIAA Paper 99-4948, November 1999.

[2]Anderson, B.H., "Design of Supersonic Inlets by a Computing Program Incorporating the Method of Characteristics," NASA TN D-4960.

[3]Cubbison, R.W., Meleason, E.T., and Johnson, D.F., "Effect of Porous Bleed in a High-Performance Axisymmetric, Mixed-Compression Inlet at Mach 2.5," NASA TMX-1692, 1968.

[4]Sanders, B.W., "Dynamic Response of a Mach 2.5 Axisymmetric Inlet and Turbojet Engine with Poppet-Valve-Controlled Inlet Stability System when Subjected to Internal and External Airflow Transients," NASA TP-1531, 1979.

[5]Saunders, J.D., and Keith, T.G., "Results from Computational Analysis of a Mixed Compression Supersonic Inlet," AIAA Paper 91-2581, June 1991. See also NASA TM-104475.

[6]Mizukami, M., and Saunders, J.D., "3D Navier-Stokes Analysis of a Mach 2.68 Bifurcated Rectangular Mixed-Compression Inlet," AIAA Paper 96-0495, January 1996.

[7]Wendt, B.J., "Suppression of Cavity-Driven Flow Separation in a Simulated Mixed Compression Inlet," NASA CR-2000-210460, September 2000.

[8]Sanders, B.W., and Weir, L.J., "2DB Inlet Test Results," Techland Report Number TR-103198, October 1998.

[9]Saunders, J.D., Frate, F.C., and Wendt, B J., "Inlet Design Methods for an X43B Demonstrator Vehicle," Paper presented at the JANNAF conference in Colorado Springs, CO. Session 4C (APS): Next Generation Launch Technology Enabling Airbreathing and Cross Cutting Technology, December 2003.

[10]Kline, S.J., Abbott, D.E., and Fox, R.W., "Optimum Design of Straight Walled Diffusers," *Journal of Basic Engineering Transactions*, ASME, Series D, 1959, pp. 321–331.

[11]McDonald, A.T., and Fox, R.W., "An Experimental Investigation of Incompressible Flow in Conical Diffusers," ASME Preprint 65-FE-25, 1965.

[12]Reneau, L.R., Johnston, J.P., and Kline, S.J., "Performance and Design of Straight Two-Dimensional Diffusers," *Journal of Basic Engineering Transactions*, ASME, Series D, 1967, pp. 141–150.

[13]Anderson, B.H., and Kapoor, K., "A Study on Bifurcated Transitioning S-Ducts for High Speed Inlet Application," AIAA Paper 94-2812, July 1994.

[14]Foster, J.D., Wendt, B.J., Reichert, B.A., and Okiishi, T.H., "Flow Through a Rectangular-to-Semiannular Diffusing Transition Duct," *Journal of Propulsion and Power*, vol. 13, no. 2, March-April 1997, pp. 312317.

[15]Coles, D.E., "Computation of Turbulent Boundary Layers," Proceedings of the AFOSRIFP-Stanford Conference, vol. II, 1968.

[16]Wendt, B.J., and Dudek, J.C., "Development of Vortex Generator Use for a Transitioning High-Speed Inlet," *Journal of Aircraft*, vol. 35, no. 4, July 1998.

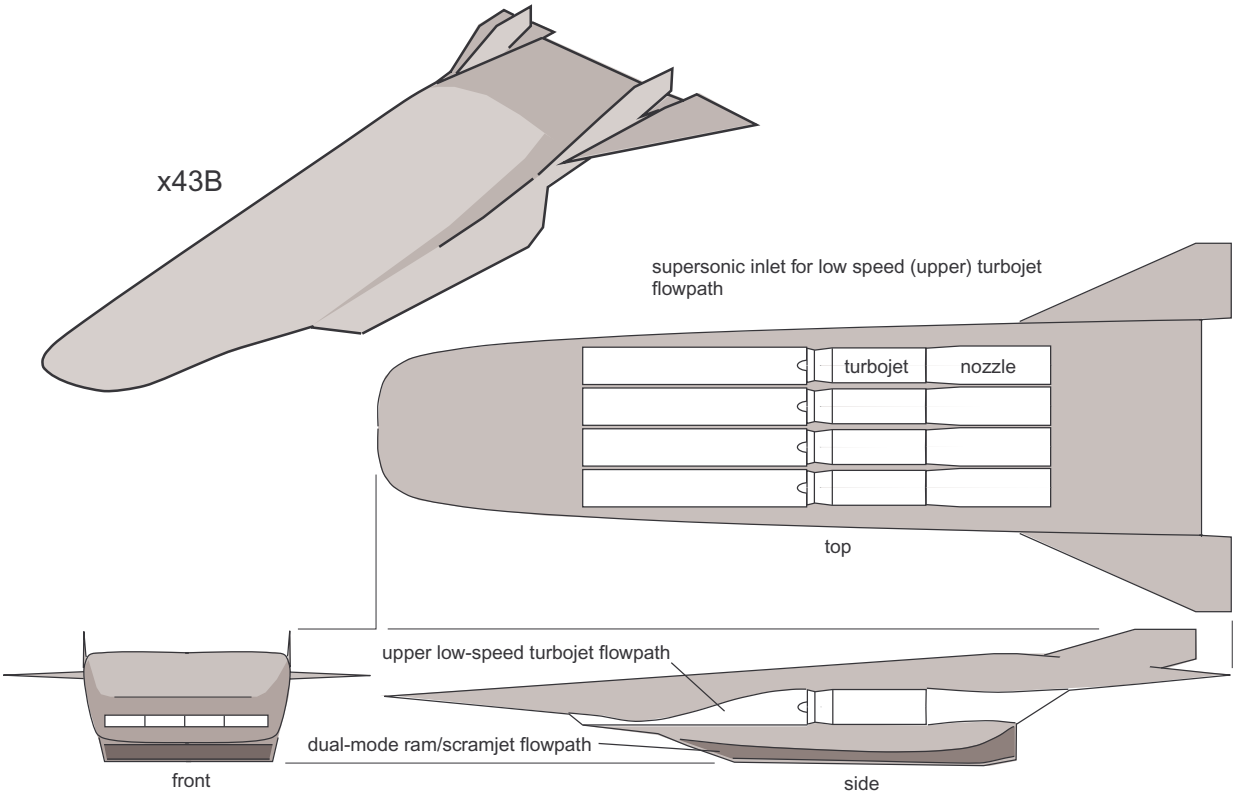

Figure 1 - Four views of the x43B. The low-speed turbojet flow path is unshaded.

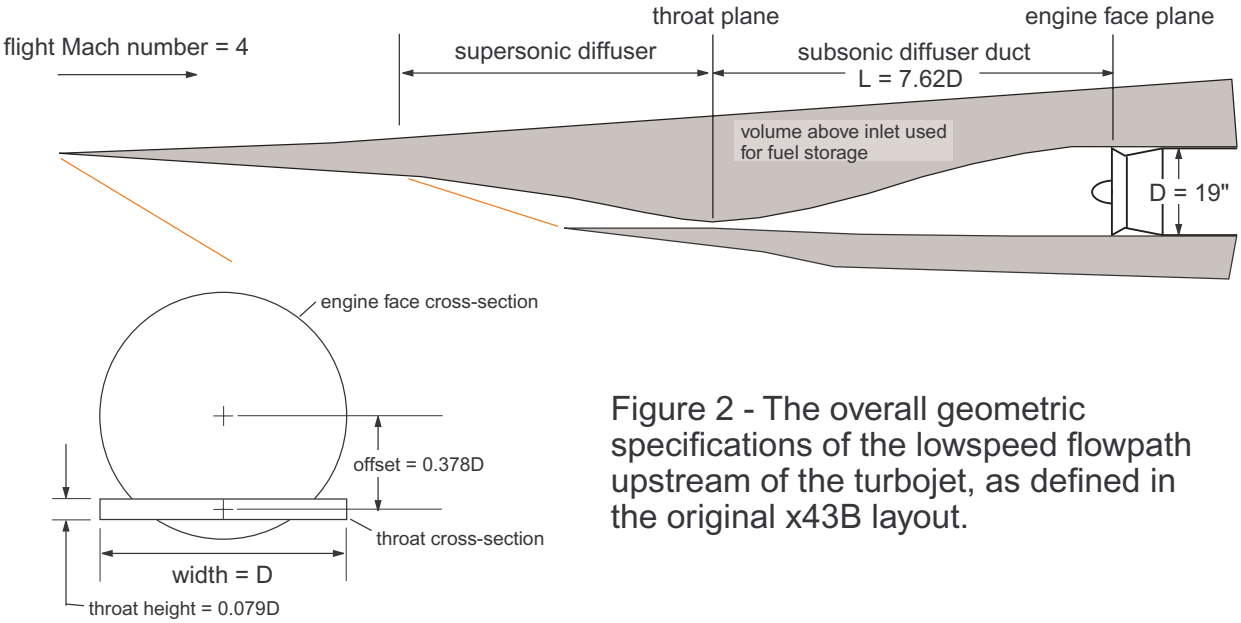

Figure 2 - The overall geometric specifications of the lowspeed flowpath upstream of the turbojet, as defined in the original x43B layout.

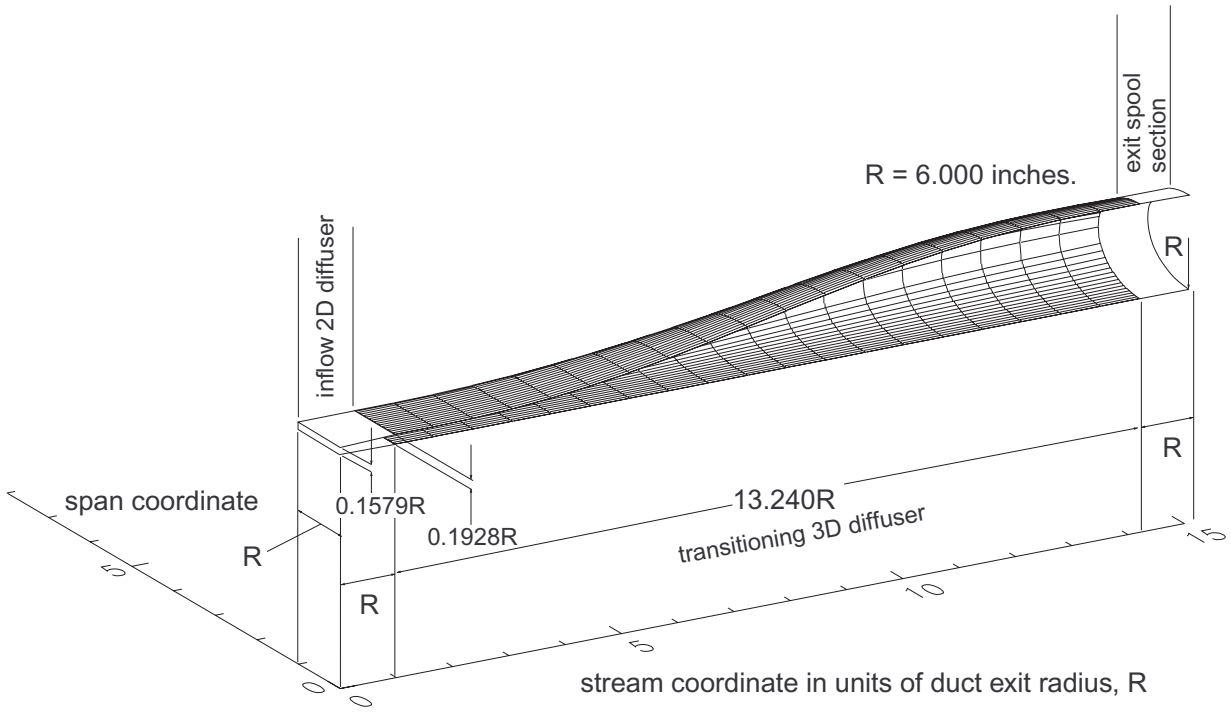

Figure 3 - An orthographic sketch of the left half of the diffuser showing the lofted surface lines. The diffuser is composed of three distinct sections; an inflow 2D diffuser, a transitioning 3D diffuser, and an exit spool section.

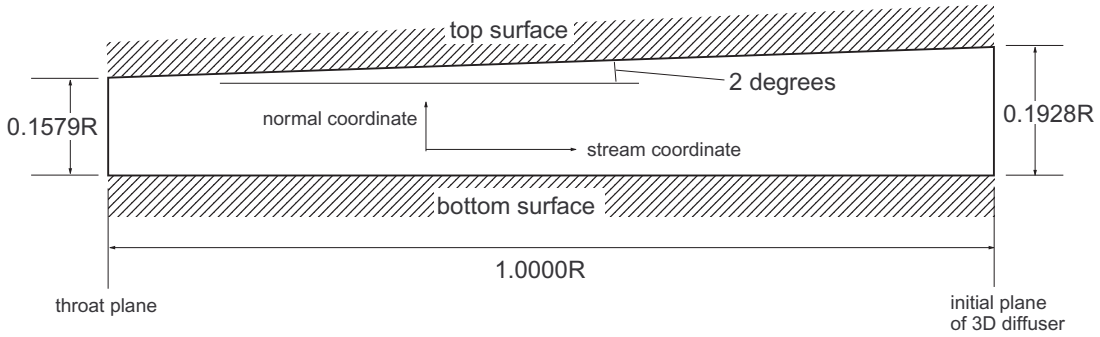

Figure 4 - A side view of the inflow 2D diffuser section.

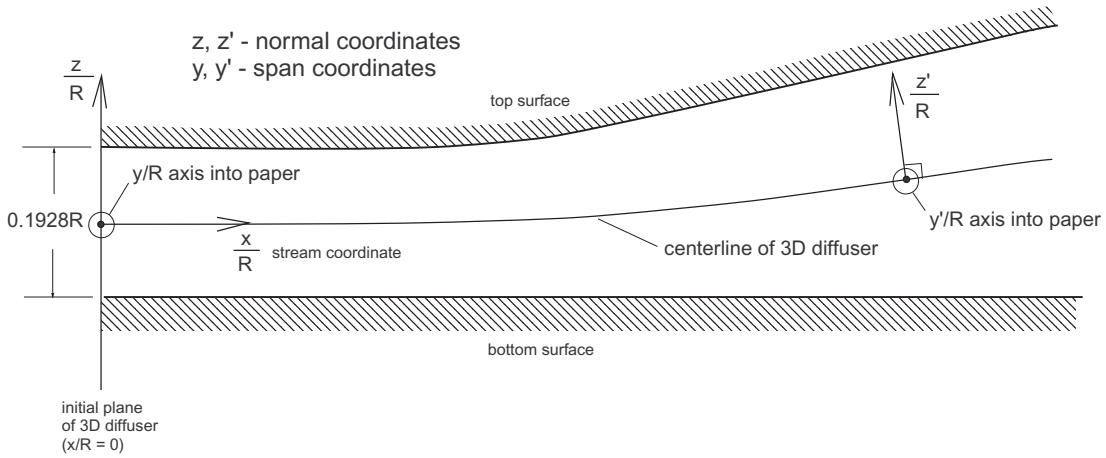

Figure 5 - The base Cartesian coordinate system and a centerline-based orthogonal coordinate system are used to define the geometry of the 3D transitioning diffuser section.

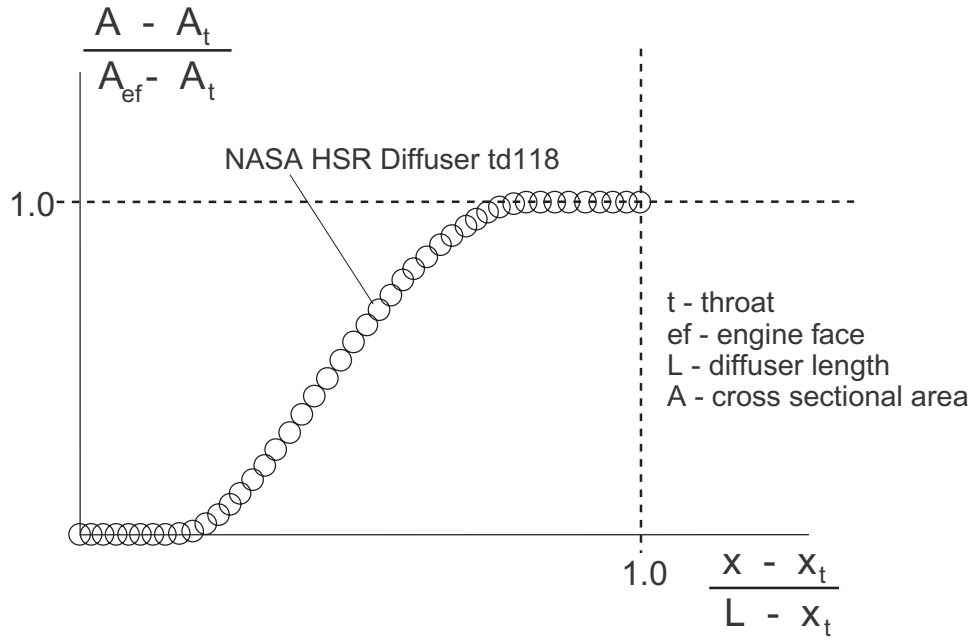

Figure 6 - The 3D transitioning diffuser section was given an area schedule identical to that of the td118 diffuser. The exponent expression, n(x/R), was adjusted iteratively (through numerical integration of Equation 2) until a precise match was obtained.

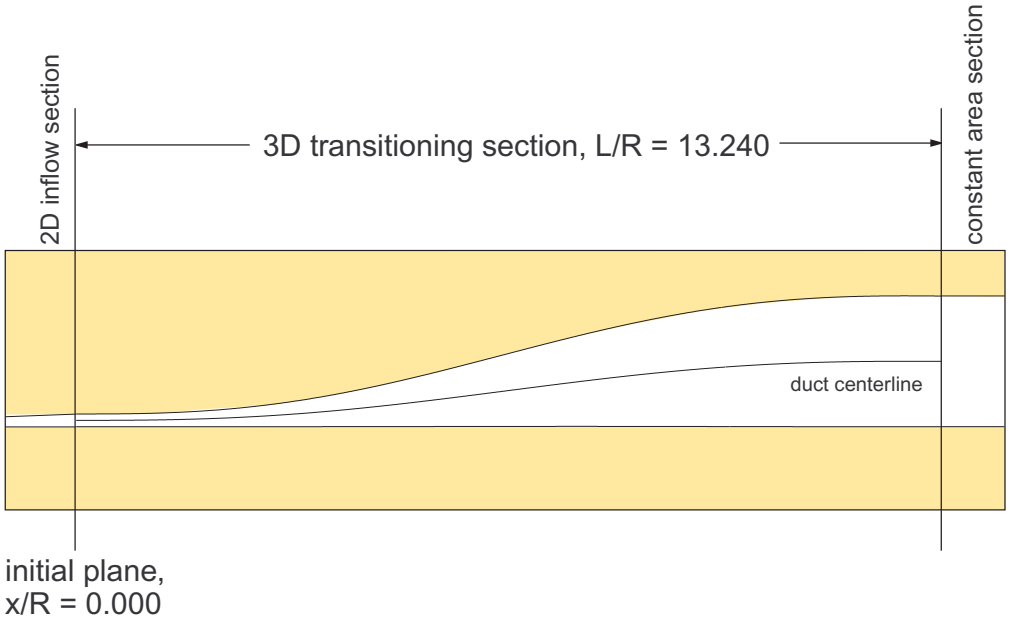

Figure 7 - An axial cut-away view of the diffuser model drawn in correct proportion.

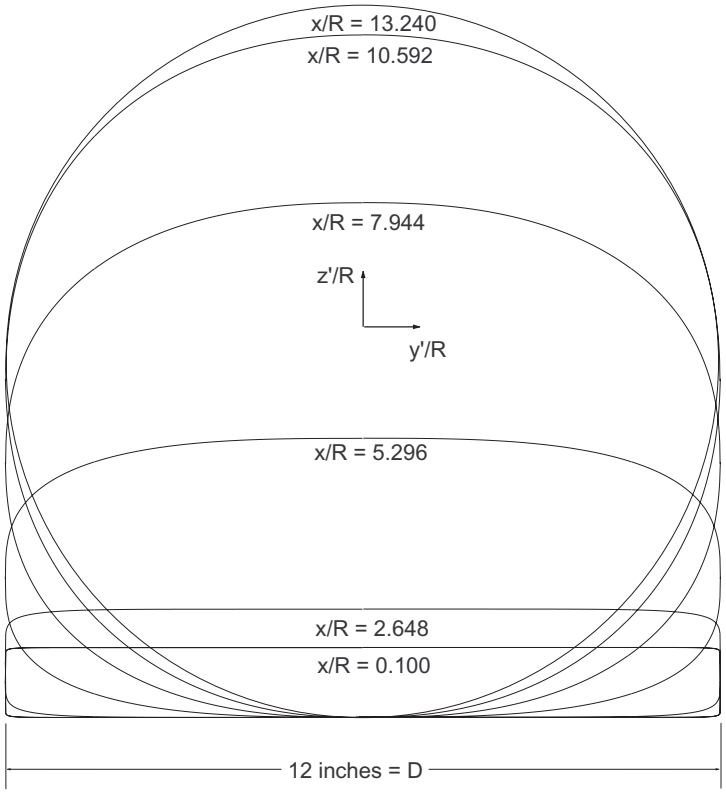

Figure 8 - Cross sections of the 3D transitioning diffuser section at six axial locations.

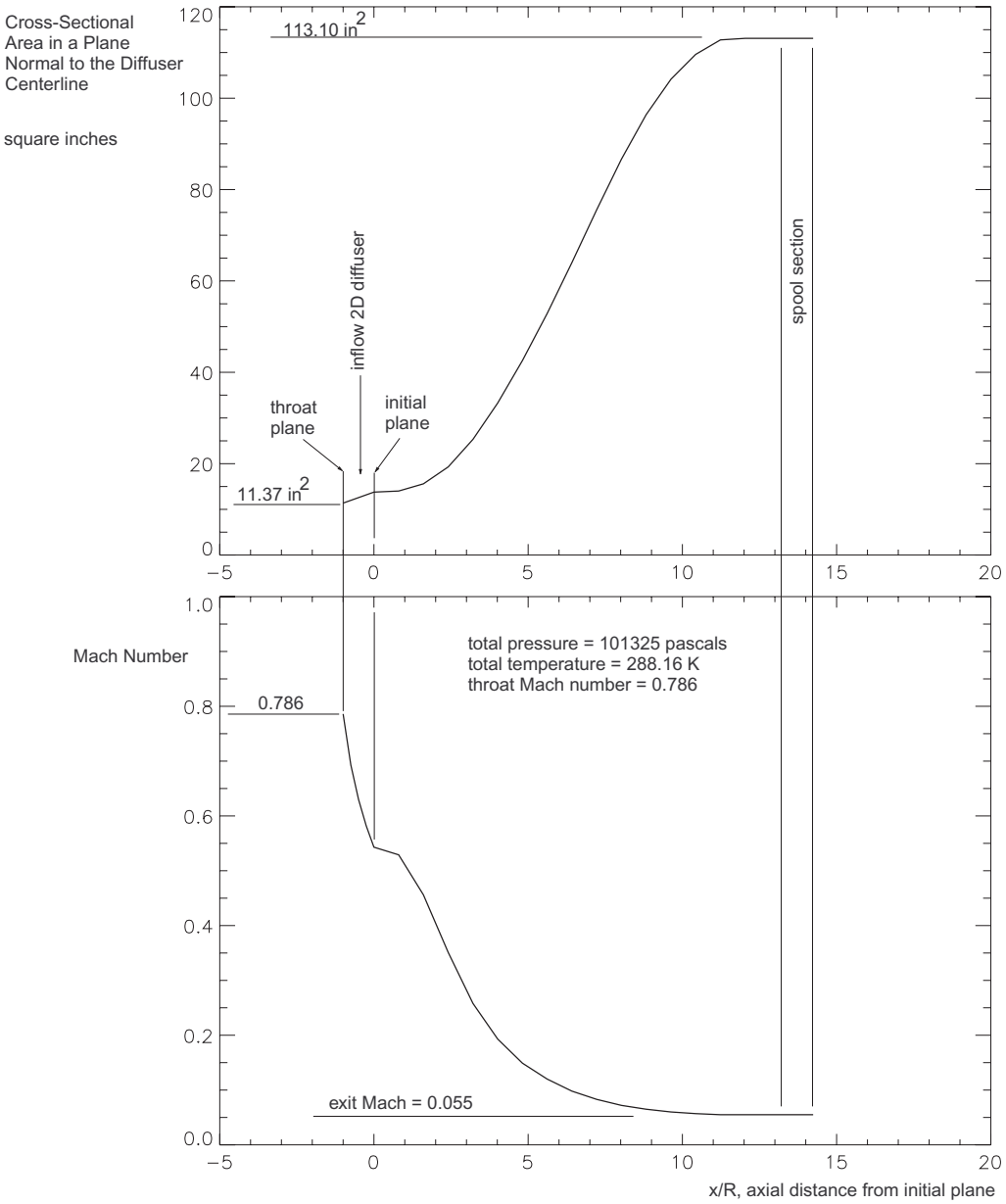

Figure 9 - Area and Mach number variation of the diffuser for given throat conditions.

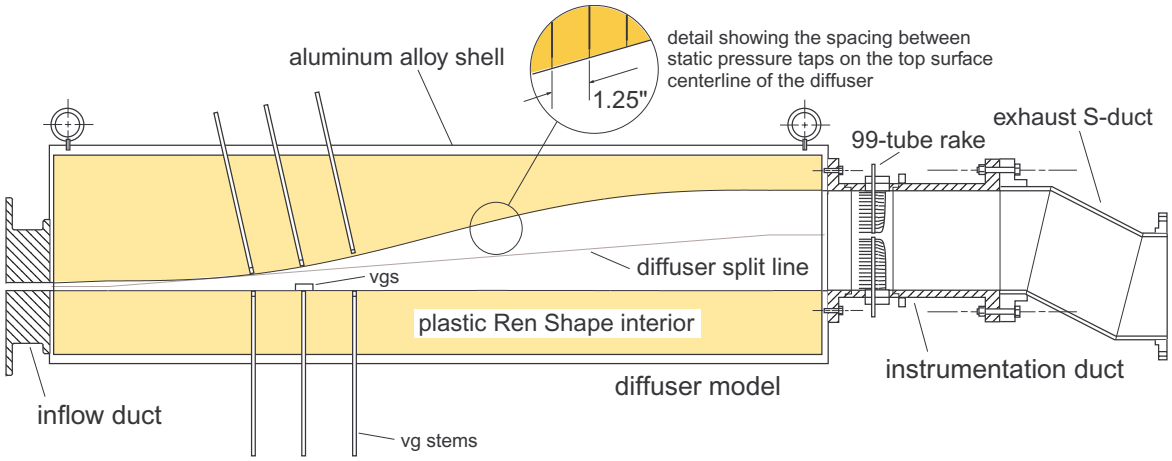

Figure 10 - An axial cut-away of the test section showing inflow duct, diffuser, and instrumentation duct.

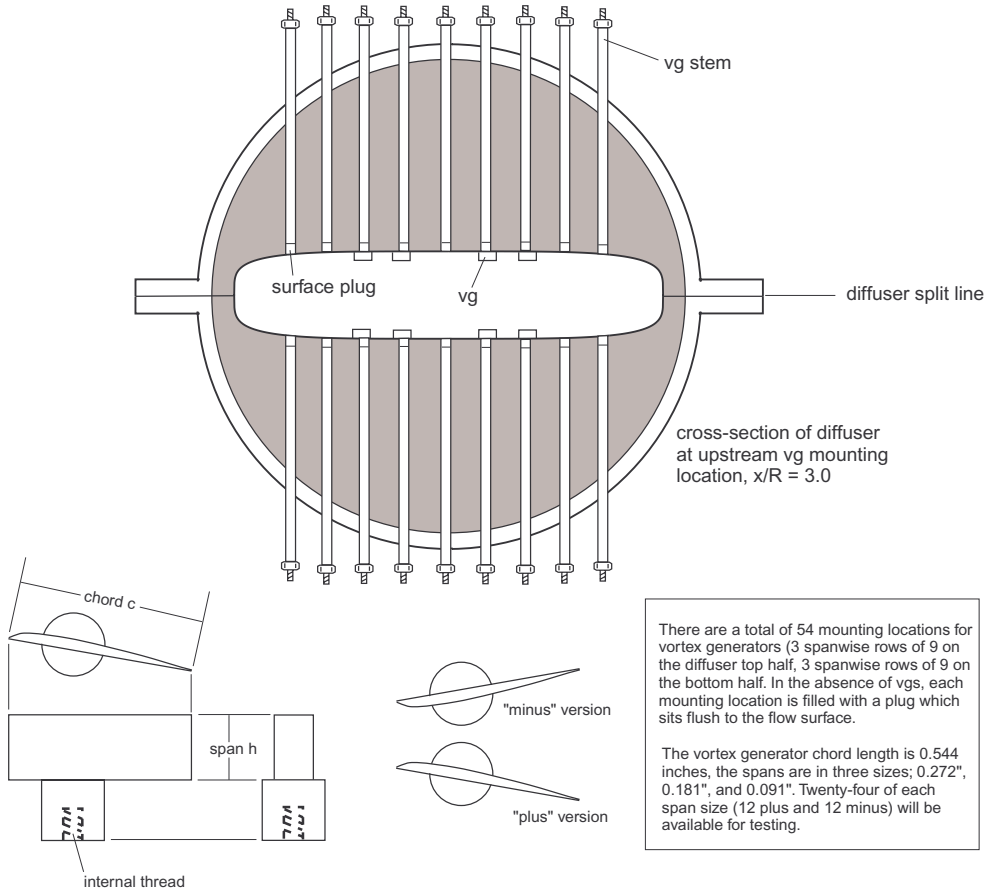

Figure 11 - A spanwise cut-away view of the diffuser showing the mounting provisions for a vortex generator array at x/R = 3.0, and the vortex generator.

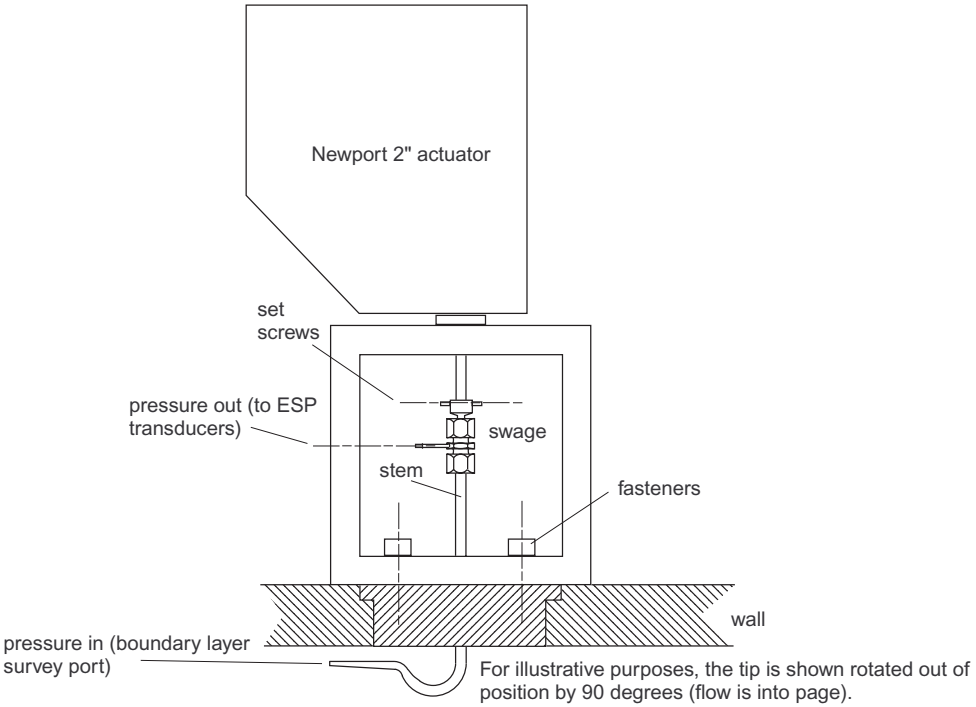

Figure 12 - The boundary layer survey system used in the inflow duct.

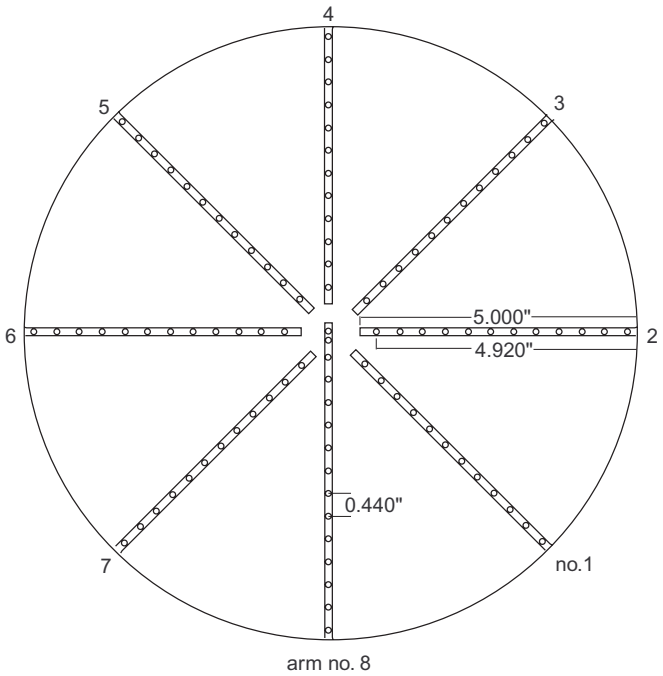

Figure 13 - The 99-tube AIP Pitot rake. Arms 1 through 7 have 12 tubes (or ports) each, arm 8 has 15 tubes.

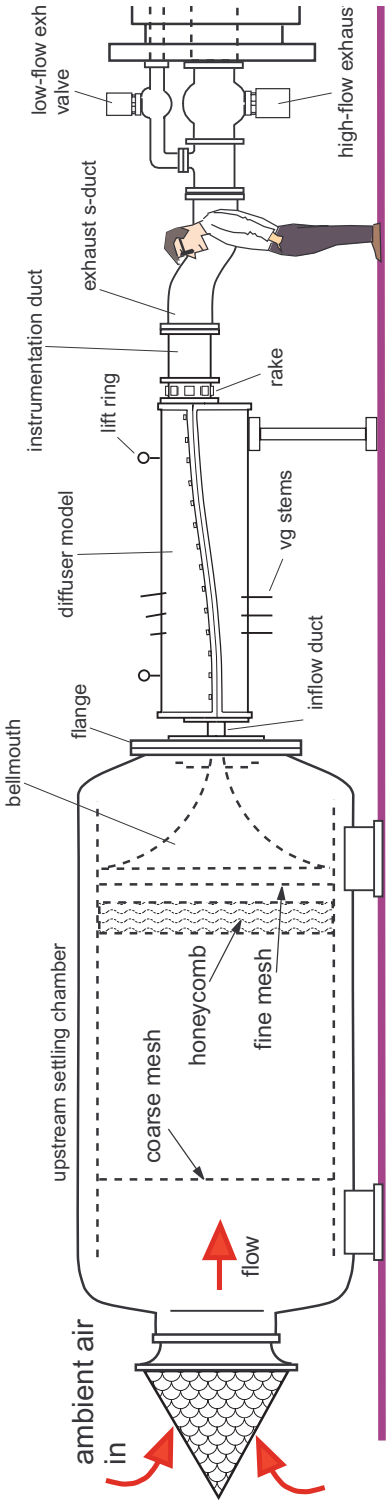

Figure 14 - The W1b facility configured for the diffuser test.

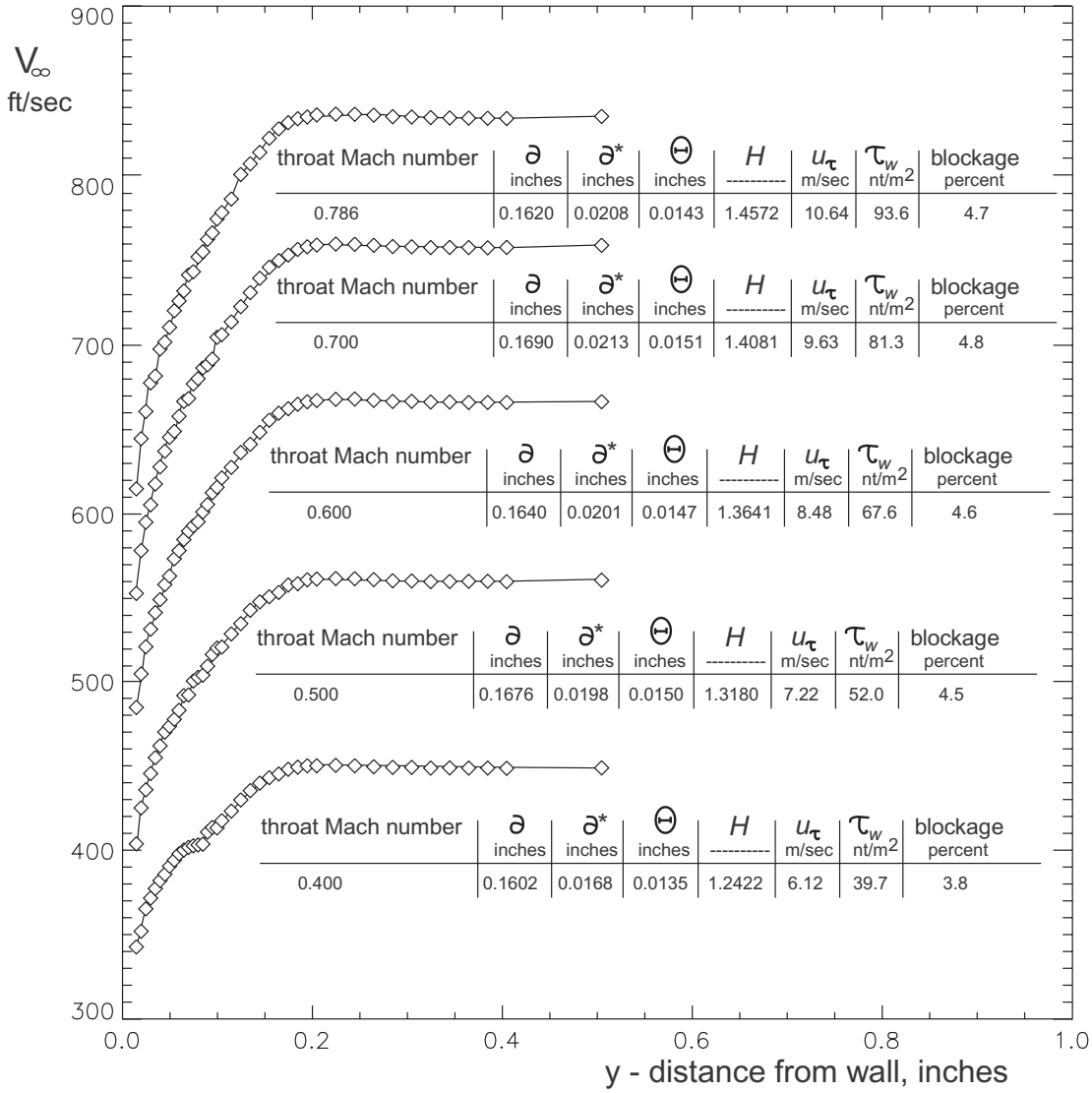

Figure 15 - Measured velocity profiles of the throat boundary layer for five throat Mach numbers.

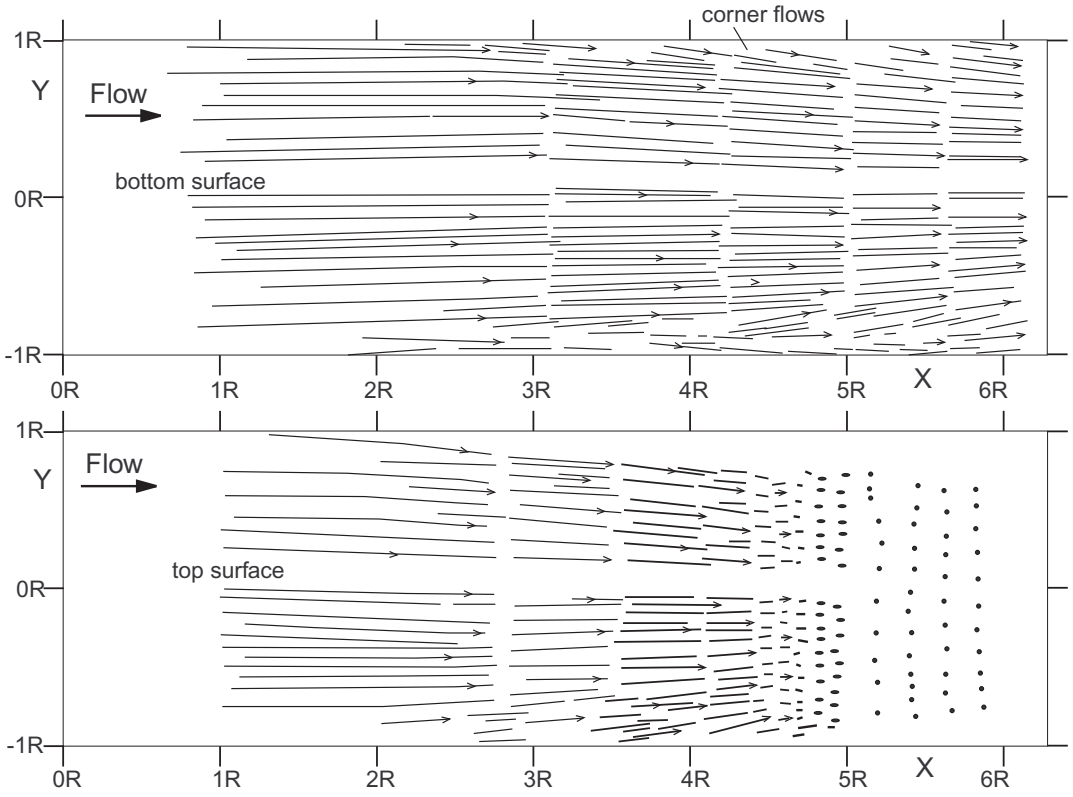

Figure 16 - Surface oil traces for the baseline diffuser in the region immediately downstream of the throat.

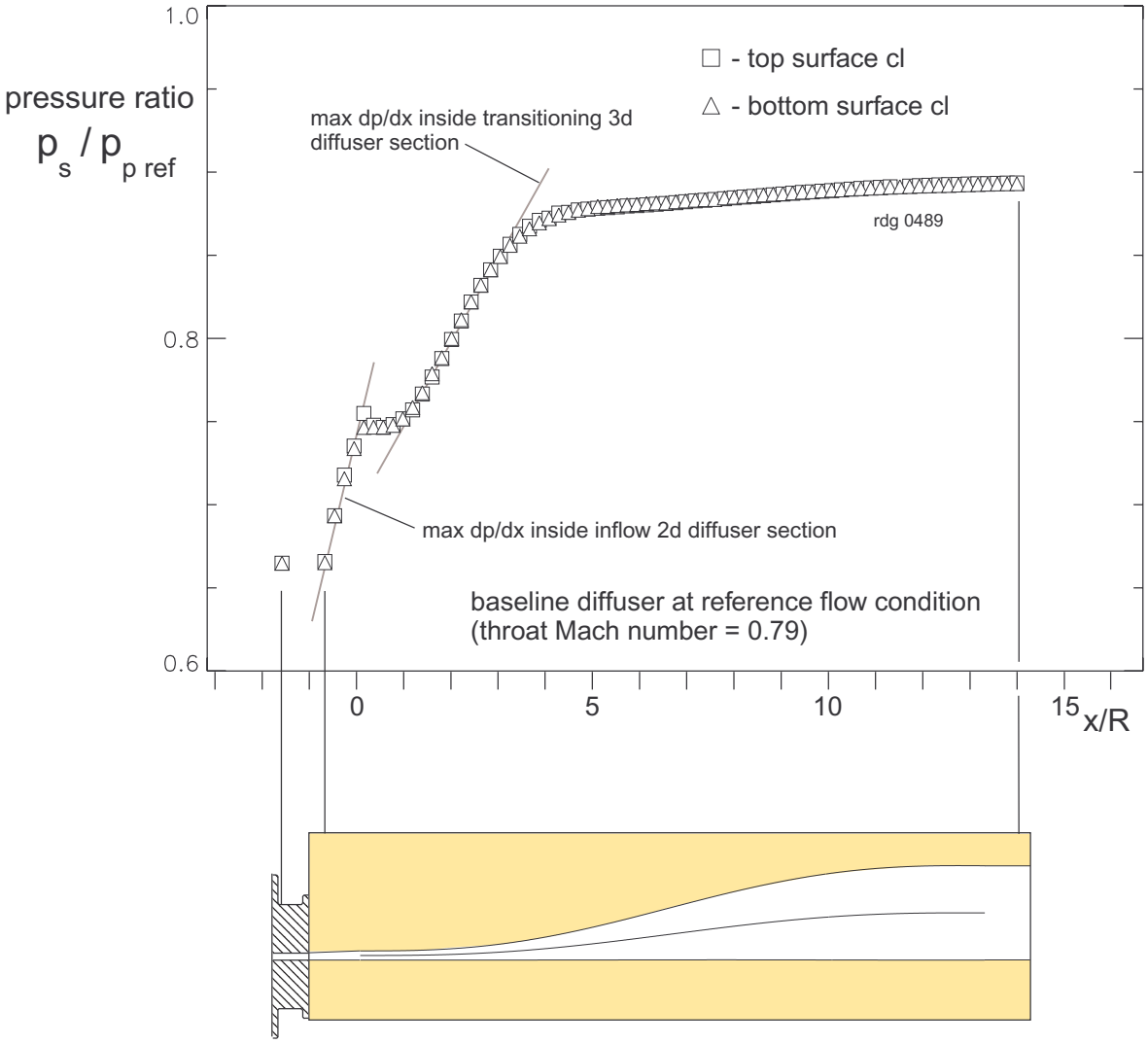

Figure 17 - Static pressure ratio axial profiles on the baseline diffuser top and bottom surface centerlines at the reference flow condition (throat Mach number = 0.79).

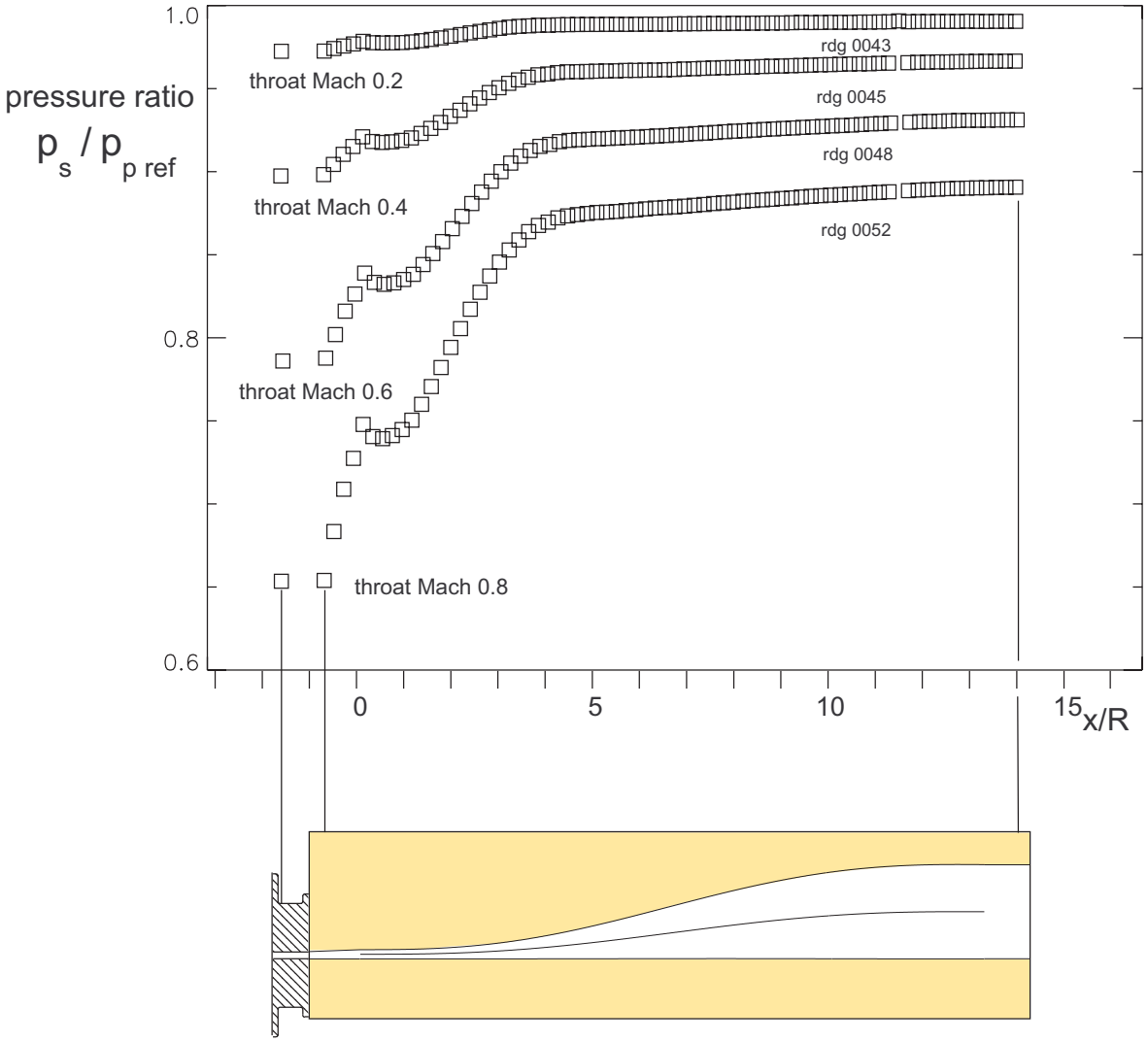

Figure 18 - Static pressure ratio axial profiles on the baseline diffuser top surface centerline for four throat Mach numbers.

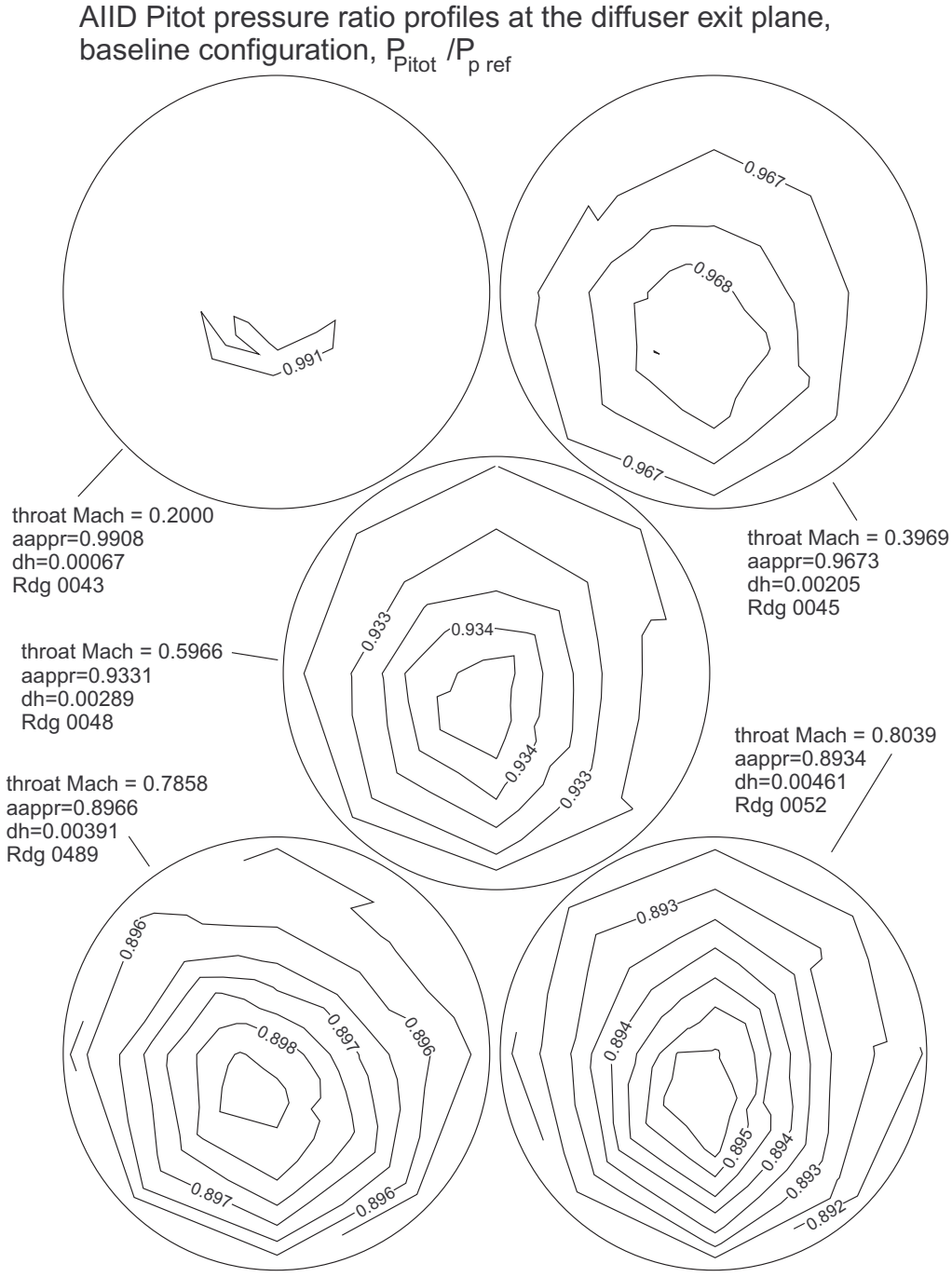

Figure 19 - AIP Pitot pressure ratio patterns and derived diffuser performance descriptors for five representative throat Mach numbers, baseline diffuser.

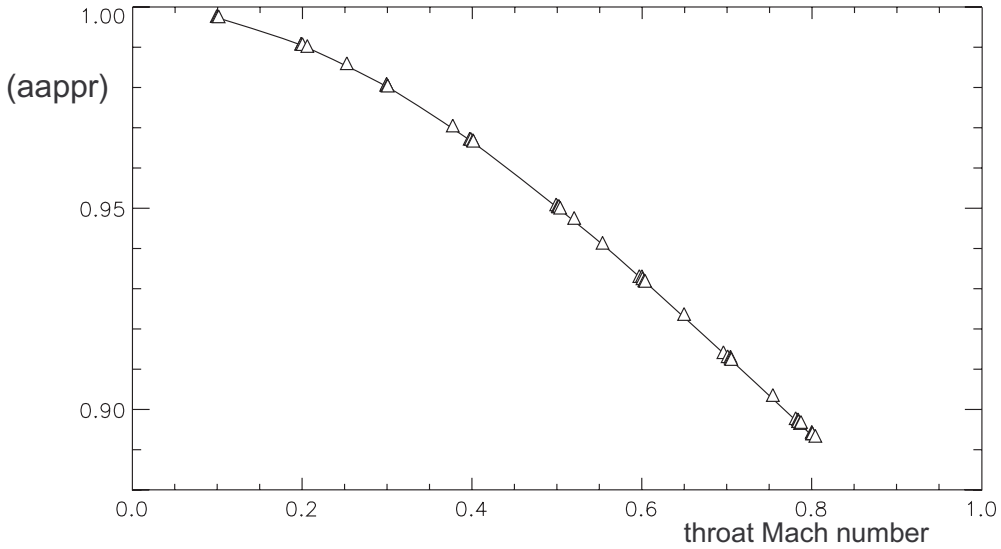

Figure 20 - Area averaged Pitot pressure recovery versus throat Mach number for the baseline diffuser.

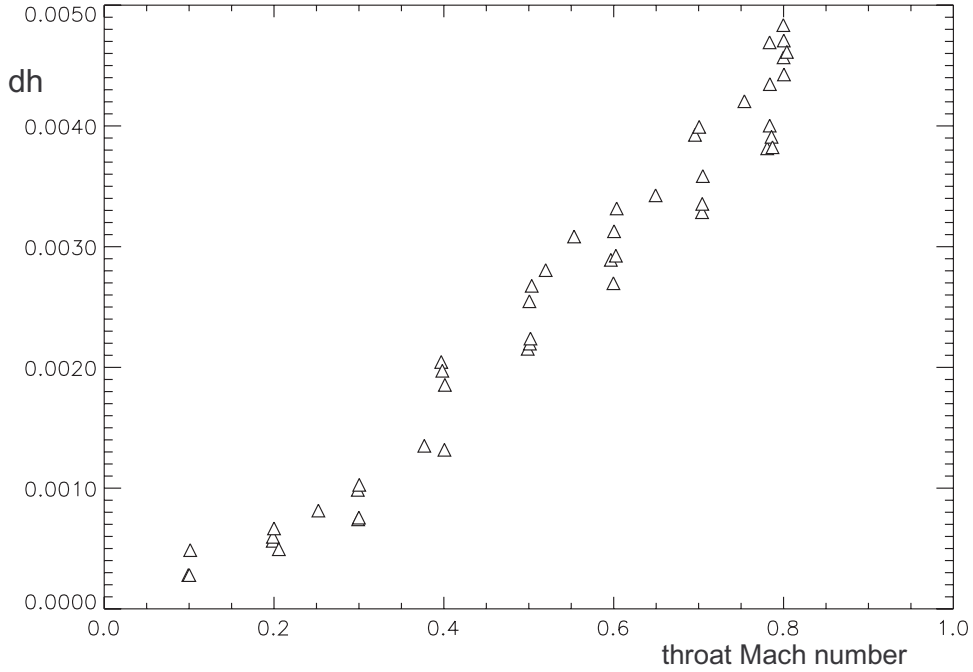

Figure 21 - The DH distortion intensity descriptor versus throat Mach number for the baseline diffuser.

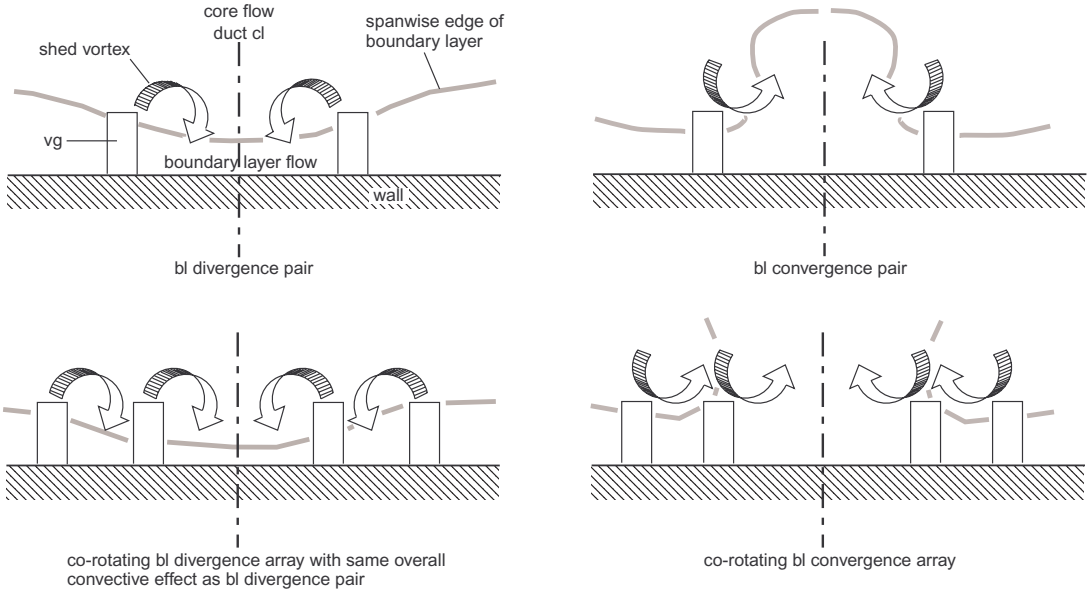

Figure 22 - A view of the vortex generator array looking downstream. The convection of the shed vortices can induce the core flow to turn in a particular direction (turn down on the left hand side, turn up on the right hand side).

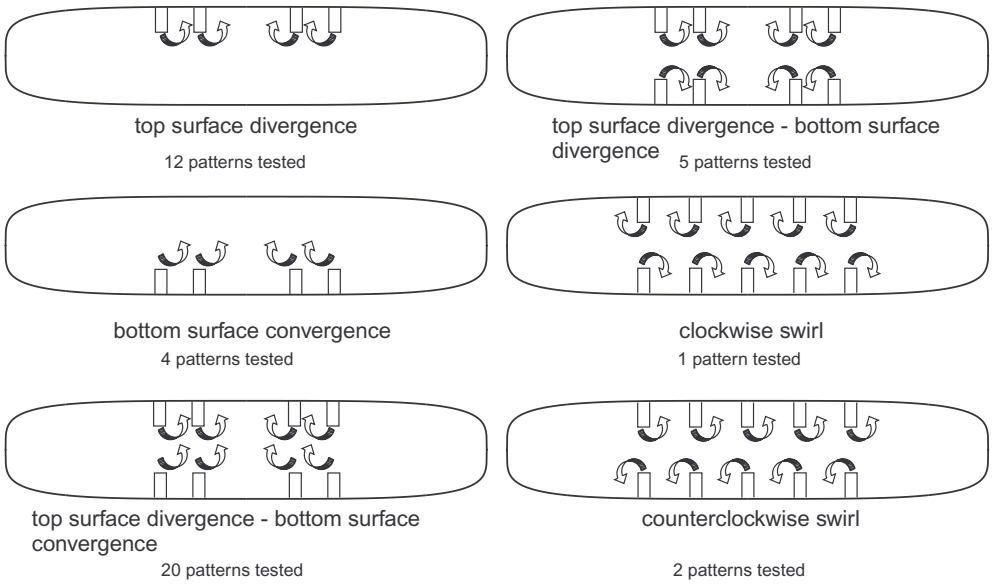

Figure 23 - A diagram of all six flow control strategies attempted in the diffuser.

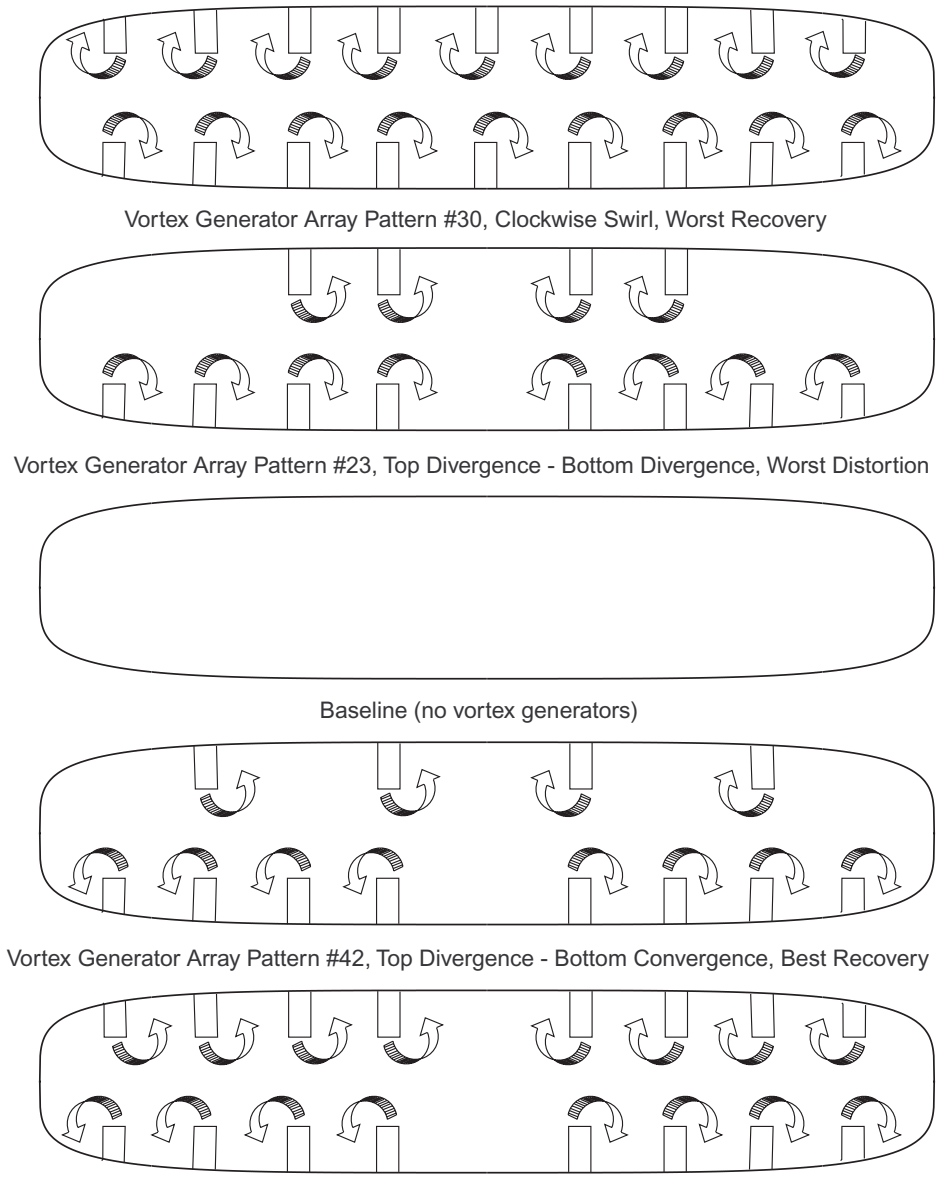

Figure 24 - Vortex generator patterns producing the worst and best AAPPR and DH distortion performance. Large vortex generators mounted at x/R = 3.0. The view is looking downstream.

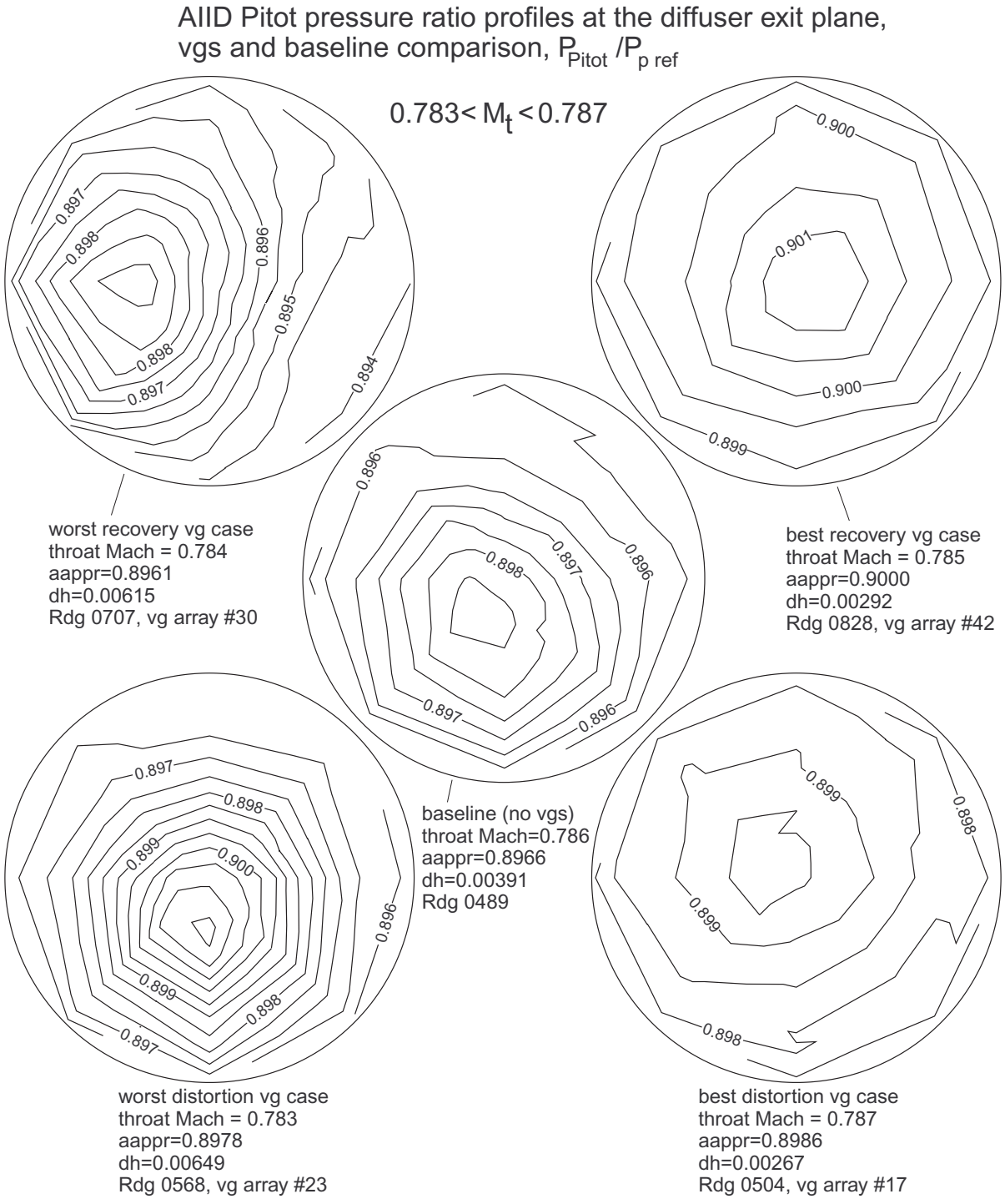

Figure 25 - AIP Pitot pressure ratio patterns and derived diffuser performance descriptors for the baseline diffuser and the diffuser configured with the best and worst performing vg arrays, near the reference throat Mach number condition.

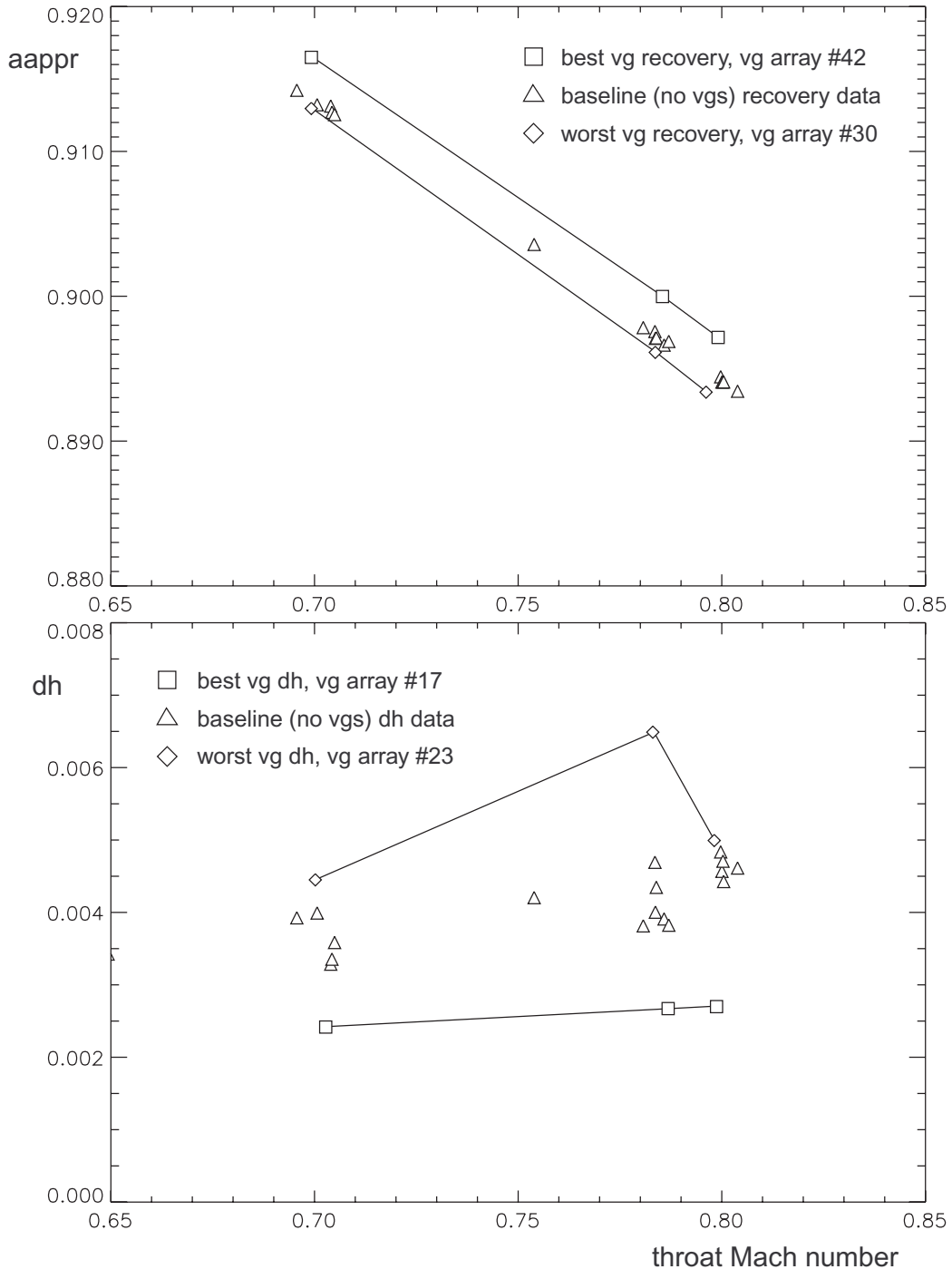

Figure 26 - A comparison of the effects of vortex generator flow control on diffuser performance.

REPORT DOCUMENTATION PAGE

Form Approved
OMB No. 0704-0188

1. AGENCY USE ONLY (*Leave blank*)	2. REPORT DATE	3. REPORT TYPE AND DATES COVERED
	December 2004	Final Contractor Report

4. TITLE AND SUBTITLE

The Performance of a Subsonic Diffuser Designed for High Speed Turbojet-Propelled Flight

5. FUNDING NUMBERS

WBS–22–090–20–C3
C80054A

6. AUTHOR(S)

Bruce J. Wendt

7. PERFORMING ORGANIZATION NAME(S) AND ADDRESS(ES)

Modern Technologies Corporation
7530 Lucerne Drive
Islander II, Suite 206
Middleburg Heights, Ohio 44130

8. PERFORMING ORGANIZATION REPORT NUMBER

E–14925

9. SPONSORING/MONITORING AGENCY NAME(S) AND ADDRESS(ES)

National Aeronautics and Space Administration
Washington, DC 20546–0001

10. SPONSORING/MONITORING AGENCY REPORT NUMBER

NASA CR—2004-213410

11. SUPPLEMENTARY NOTES

Bruce J. Wendt, Modern Technologies Corporation, Middleburg Heights, Ohio 44130 and NASA Resident Research Associate at Glenn Research Center. Project Manager, Thomas J. Biesiadny, Turbomachinery and Propulsion Systems Division, NASA Glenn Research Center, organization code RTL, 216–433–3967.

12a. DISTRIBUTION/AVAILABILITY STATEMENT

Unclassified - Unlimited
Subject Category: 02 Distribution: Nonstandard

Available electronically at http://gltrs.grc.nasa.gov

This publication is available from the NASA Center for AeroSpace Information, 301–621–0390.

12b. DISTRIBUTION CODE

13. ABSTRACT ***(Maximum 200 words)***

An initial-phase subsonic diffuser has been designed for the turbojet flowpath of the hypersonic x43B flight demonstrator vehicle. The diffuser fit into a proposed mixed-compression supersonic inlet system and featured a cross-sectional shape transitioning flowpath (high aspect ratio rectangular throat-to-circular engine face) and a centerline offset. This subsonic diffuser has been fabricated and tested at the W1B internal flow facility at NASA Glenn Research Center. At an operating throat Mach number of 0.79, baseline Pitot pressure recovery was found to be just under 0.9, and DH distortion intensity was about 0.4 percent. The diffuser internal flow stagnated, but did not separate on the offset surface of this initial-phase subsonic diffuser. Small improvements in recovery (+0.4 percent) and DH distortion (–32 percent) were obtained from using vane vortex generator flow control applied just downstream of the diffuser throat. The optimum vortex generator array patterns produced inflow boundary layer divergence (local downwash) on the offset surface centerline of the diffuser, and an inflow boundary layer convergence (local upwash) on the centerline of the opposite surface.

14. SUBJECT TERMS

Engine inlets; Inlet flow; Diffusers; Hypersonic inlets

15. NUMBER OF PAGES

33

16. PRICE CODE

17. SECURITY CLASSIFICATION OF REPORT	18. SECURITY CLASSIFICATION OF THIS PAGE	19. SECURITY CLASSIFICATION OF ABSTRACT	20. LIMITATION OF ABSTRACT
Unclassified	Unclassified	Unclassified	